



Lawrence Berkeley National Laboratory

Earth & Environmental Sciences Area



6 September 2018

Dear Dr. Kala,

My co-authors and I are pleased to submit revised manuscript entitled "*Development and evaluation of a variably saturated flow model in the global E3SM Land Model (ELM) Version 1.0*" for your consideration as a model description paper in *Geoscientific Model Development*.

We very much appreciate the reviewers' comments and feel that they have allowed us to substantially improve our manuscript. Modifications made in the revised version of the manuscript as compared to the last submission are summarized below:

1. We performed additional new 10-years simulations to demonstrate robustness numerical solutions with respect to spatial and temporal resolutions. We have added description of new simulation results to the Supplemental Material, and describe them in the revised Results section.
2. As suggested by reviewer-2, we added additional details on the time integration methodology of the model in the Appendix.
3. Finally, we have provided detailed response to all comments from the two reviewers.

My co-authors and I believe we have thoroughly addressed all the reviewer comments and that the revised manuscript is well suited for publication in *Geoscientific Model Development*. We look forward to receiving your response.

Sincerely,
Gautam Bisht

Lawrence Berkeley National Laboratory

Reviewer #1

(1) Eq. (10) - typically P_c is compared against air entry pressure instead of 0.

Response:

Equation 10 has been corrected following the reviewer's suggestion.

(2) Not all variables are defined in Eq. (10) and (11).

Response:

Definitions of missing variables have been now added in the latest version of the manuscript.

(3) Variables in Eq. (16) defined in the appendix, but not in the main text.

Response:

Definition of missing variables have been now added in the latest version of the manuscript.

(4) Redundant "nonlinear" in line 221.

Response:

The text has been updated to remove the redundant 'nonlinear'.

(5) I don't agree with the statement in lines 233 to 234. At least one can compare water table depth and soil moisture using VFSM and the default scheme within ELM.

Response:

In ELMv0, code for individual process models cannot be built independent of E3SM code base. Thus, individual process models cannot be easily tested against analytical solutions or other model configurations. We have updated the text to clarify this ELMv0 limitation.

(6) It's not clear which WRC is used for the tests from Table 1 as parameters from both Eqs. 10 and (11) are used. From line 255, Van Genuchten model is used, then n and m are missing in

Response:

All three test problems used the van Genuchten model. The second column of Table 1 originally incorrectly listed values for 'lambda' instead of 'm'. Table 1 has been corrected and the equation for computing 'n' based on 'm' has been added on line 201.

Table 1.

(9) line 298 - what is beta?

Response:

Beta [radians] is mean grid cell topographic slope and is now described in the updated text.

Report #2

1. The authors tried to demonstrate the robustness of ELMv1-VSFM by conducting several experimental simulations. However, there may be inaccuracies in numerical solutions due to differences in the size of spatial and temporal mesh (El-Kadi & Ling, 1993). The authors used outputs from simulations with different configurations (e.g. spatial resolution of grid-cell, soil column depth, spatial discretization) to support the robustness of global analysis. Moreover, temporal resolutions used in the experimental simulations are not indicated in the paper. Since information required for ensuring numerical stability of the model is not indicated, I am not sure whether or not ELMv1-VSFM converges well at a spatial-temporal resolution of 1.90 (latitude) × 2.50 (longitude) with a 30 [min] time-step.

Response:

We have now updated Table 1 to include information about the spatial and temporal discretization used for the three single-column benchmark problems. Additionally, Section 3.1 has been updated to include a reference to Table 1. To address the reviewer's comment regarding numerical stability, we performed simulations with higher vertical and temporal resolution, as described below in our responses to Reviewer #2.

2. The authors mentioned that there are advantages to using variably-saturated flow model (variably saturated Richards' equation) rather than applying different governing equations for each flow domain noted in the previous work. However, they did not specify what the relative strengths of using variably saturated Richards' equation are compared to adapting different equations (e.g., computational cost). The reason why they intended to unify the treatment of soil hydrologic processes should be stated.

Response:

Clark et al. (2015) summarized opportunities and challenges for improving hydrological processes in the global land surface models and identified that incorporation of variably saturated hydrologic flow models is expected to improve simulation of coupled soil moisture and shallow groundwater dynamics. In the last version of our manuscript, the reference to the Clark et al. (2015) study was included in the Introduction section. In order to state the motivation of our work upfront, we have updated the abstract to include reference to Clark et al. (2015) recommendation for developing a unified treatment of soil hydrologic processes.

3. The authors used ILAMB package to show additional consideration of saturated zone does not degrade the model's predictive capabilities in other hydrologic processes. However, without any explanation of the interaction between groundwater and other components (e.g., streamflow, LH/SH), it is difficult to accept the author's claim saying further consideration about groundwater- surface water interaction does not degrade other predictions.

Response:

As stated in the revised manuscript starting on line 412, “The International Land Model Benchmarking (ILAMB) package (Hoffman et al., 2017) provides a comprehensive evaluation of predictions of carbon cycle states and fluxes, hydrology, surface energy budgets, and functional relationships by comparison to a wide range of observations”. The ILAMB package explicitly compares model predictions of many hydrological and surface energy components, including large river basin flows, LH, SH, etc. In the revised manuscript, Table 3 compares bias, RMSE, and an ILAMB score (which combines metrics associated with spatial and temporal variability, biases, etc.) for LH, SH, TWSA, and large river basin flows.

4. The authors mentioned this work has a focus on representing groundwater-surface water interactions but all the outputs appear to be related addressing subsurface hydrology using VSFM. The authors may want to specify what they did to emphasize their focus on groundwater-surface water interactions by adding more results regarding that (e.g., interactive effect between runoff and groundwater level)

Response:

The work we report on here focuses on improving near-surface soil moisture and ground hydrology representation in ELM. We have corrected the abstract in the revised manuscript to clarify this point.

I would like to note some recommendations for this paper:

- 6) how the authors determine the robustness of the model based on the results of the experimental simulations should be specified.*

Response:

In order to demonstrate model robustness and flexibility to easily configure the model for a range of problem setups, we performed VSFM simulations for three offline simulation as described in Section 2.3. The problems included infiltration in a dry soil column, infiltration in a layered soil system, and water table dynamics in a variably saturated soil column. For all three problems, VSFM results accurately reproduced published datasets and agreed well with predictions from an existing variably saturated flow model. The benchmark problems used in our study have been previously used to show robustness of variably saturated flow models (Kumar et al., 2009; Shen and Phanikumar, 2010).

2) the authors may need to perform experimental simulations with the same configuration used for global analysis in order to show the numerical stability of the model.

Response:

Since there is such a large mismatch in temporal (days versus 100's of years) and spatial (2 m versus 150 m deep) scales between the benchmark problems and global simulations, we do not believe it is appropriate to perform 1D benchmark simulations with the spatio-temporal configurations of global simulations. However, we acknowledge that the reviewer has a valid concern about the sensitivity of numerical solutions with respect to spatial and temporal

resolutions. Therefore, to address this issue, we performed the following additional new 10-years simulations:

1. SIM_HALF_DT: All configurations were the same as those used in the global simulation with optimal f_d except maximum allowable VSFM timestep was set to 15 min
2. SIM_HALF_DT_AND_HALF_DZ: All configurations were the same as those used in the global simulation with optimal f_d except maximum allowable VSFM timestep was set to 15 min and spatial resolution of ELM was doubled by increasing the number of soil layers to 118 and decreasing the soil thickness for each layer appropriately to keep the total soil column depth fixed at 150 m.

The results are encouraging: the global mean difference in the simulated annual water table depth (WTD) for the 10th year between SIM_OPT and SIM_HALF_DT at 25th, 50th, and 75th percentiles were extremely small (0.001, 0.002 and 0.005 m, respectively). Small difference between SIM_OPT and SIM_HALF_DT_AND_HALF_DZ at 25th, 50th, and 75th percentiles were also found (0.091, 0.488, 0.945 [m], respectively). These results show that simulated WTD is insensitive to VSFM sub timestep, and has small sensitivity to vertical spatial resolution. We have added these simulation results to the Supplemental Material, and describe them in the revised Results section.

3) the authors may want to demonstrate the numerical stability of the model by providing some indexes (e.g., Peclet number).

Response:

We thank the reviewer for this suggestion, as including more details on numerical properties of the model will improve the manuscript. VSFM uses a two-stage check to determine an acceptable numerical solution:

- Stage-1: At any temporal integration stage, the model attempts to solve the set of nonlinear equations given by Equation 19 with a given timestep. If the model fails to find a solution to the nonlinear equations with a given error tolerance settings, the timestep is reduced by half and the model again attempts to solve the nonlinear problem. If the model fails to find a solution after a maximum number of time step cuts (currently 20), the model reports an error and stops execution. None of the simulations reported in this paper failed this check.
- Stage-2: After a numerical solution for the nonlinear problem is obtained, a mass balance error is calculated as the difference between input and output fluxes and change in mass over the integration timestep. If the mass balance error exceeds 10^{-5} kg m⁻², the error tolerances for the nonlinear problem are tightened by a factor of 10 and the model re-enters Stage-1. If the model fails to find a solution with an acceptable mass balance error after 10 attempts of tightening error tolerances, the model reports an error and stops execution. None of the simulations reported in this paper failed this check.

We extended the Appendix to include a new section, 5.4, to details about the time integration methodology of VSFM, as described above.

4) *the authors can demonstrate the benefits of applying variably-saturated flow model compared to outputs derived from different physics application, especially in terms of computational cost.*

Response:

As described in Section 3.3 of the manuscript, we performed computational cost calculations for VSFM using 96, 192, 384, 768, and 1536 cores. Compared to the default hydrological model, VSFM is ~30% more expensive on an optimal processor layout. To address this reviewer comment, we have additionally added a figure showing the performance of the default model and VSFM at different core counts in Supplementary material.

5) *the authors may want to add some description about the modeling scheme used for representing the interactions between stream and groundwater and between evapotranspiration and groundwater.*

Response:

VSFM does not explicitly represent stream and groundwater interactions. VSFM is driven by a vertically prescribed source/sink of water over the soil column, which has been calculated by other components of ELM (e.g., transpiration, infiltration). Section 2.2 has been updated to describe how all sources and sinks of water are handled in VSFM.

6) *To emphasize their motivation for groundwater-surface water interaction, the authors may want to indicate how runoff simulation is correlated groundwater level.*

Response:

As indicated in Table 3, runoff (which includes subsurface and surface components) does depend on groundwater depth, and globally the change in the ILAMB score using default and optimal drainage parameter is only 0.02 m. As mentioned above in response to reviewer #1's comment, the focus of this work is on near-surface soil moisture and GW, and not on effects to surface water dynamics. We have clarified this point in the Abstract and Introduction of the revised manuscript.

References

Clark, M. P., Fan, Y., Lawrence, D. M., Adam, J. C., Bolster, D., Gochis, D. J., Hooper, R. P., Kumar, M., Leung, L. R., Mackay, D. S., Maxwell, R. M., Shen, C., Swenson, S. C., and Zeng, X.: Improving the representation of hydrologic processes in Earth System Models, *Water Resources Research*, 51, 5929-5956, 2015.

Hoffman, F. M., Koven, C. D., Keppel-Aleks, G., Lawrence, D. M., Riley, W. J., Randerson, J. T., Ahlstrom, A., Abramowitz, G., Baldocchi, D. D., Best, M. J., Bond-Lamberty, B., Kauwe}, M. G. D., Denning, A. S., Desai, A. R., Eyring, V., Fisher, J. B., Fisher, R. A., Gleckler, P. J., Huang, M., Hugelius, G., Jain, A. K., Kiang, N. Y., Kim, H., Koster, R. D., Kumar, S. V., Li, H., Luo, Y., Mao, J., McDowell, N. G., Mishra, U., Moorcroft, P. R., Pau, G. S. H., Ricciuto, D. M., Schaefer, K., Schwalm, C. R., Serbin, S. P., Shevliakova, E., Slater, A. G., Tang, J., Williams, M., Xia, J., Xu, C., Joseph, R., and Koch, D.: International Land Model

Benchmarking (ILAMB) 2016 Workshop Report, U.S. Department of Energy, Office of Science, 159 pp., 2017.

Kumar, M., Duffy, C. J., and Salvage, K. M.: A Second-Order Accurate, Finite Volume-Based, Integrated Hydrologic Modeling (FIHM) Framework for Simulation of Surface and Subsurface Flow, *Vadose Zone Journal*, 8, 873-890, 2009.

Shen, C. and Phanikumar, M. S.: A process-based, distributed hydrologic model based on a large-scale method for surface–subsurface coupling, *Advances in Water Resources*, 33, 1524-1541, 2010.

1 **Development and evaluation of a variably saturated flow model in the global**
2 **E3SM Land Model (ELM) Version 1.0**

3

4 **Gautam Bisht¹, William J. Riley¹, Glenn E. Hammond², and David M. Lorenzetti³**

5

6 ¹Climate & Ecosystem Sciences Division, Lawrence Berkeley National Laboratory,1
7 Cyclotron Road, Berkeley, California 94720, USA

8

9 ²Applied Systems Analysis and Research Department, Sandia National Laboratories,
10 Albuquerque, NM 87185-0747, USA

11

12 ³Sustainable Energy Systems Group, Lawrence Berkeley National Laboratory,1
13 Cyclotron Road, Berkeley, California 94720, USA

14

15 Correspondence to: Gautam Bisht (gbisht@lbl.gov)

16 **Abstract**

17 Improving global-scale model representations of near-surface soil moisture and
18 groundwater hydrology is important for accurately simulating terrestrial processes
19 and predicting climate change effects on water resources. Most existing land surface
20 models, including the default E3SM Land Model (ELMv0), which we modify here,
21 routinely employ different formulations for water transport in the vadose and
22 phreatic zones. Clark et al. (2015) identified a variably saturated Richards equation
23 flow model as an important capability for improving simulation of coupled soil
24 moisture and shallow groundwater dynamics. In this work, we developed the
25 Variably Saturated Flow Model (VSFM) in ELMv1 to unify the treatment of soil
26 hydrologic processes in the unsaturated and saturated zones. VSFM was tested on
27 three benchmark problems and results were evaluated against observations and an
28 existing benchmark model (PFLOTRAN). The ELMv1-VSFM's subsurface drainage
29 parameter, f_d , was calibrated to match an observationally-constrained and spatially-
30 explicit global water table depth (WTD) product. Optimal spatially-explicit f_d values
31 were obtained for 79% of global $1.9^0 \times 2.5^0$ gridcells, while the remaining 21% of
32 global gridcells had predicted WTD deeper than the observationally-constrained
33 estimate. Comparison with predictions using the default f_d value demonstrated that
34 calibration significantly improved predictions, primarily by allowing much deeper
35 WTDs. Model evaluation using the International Land Model Benchmarking package
36 (ILAMB) showed that improvements in WTD predictions did not degrade model skill
37 for any other metrics. We evaluated the computational performance of the VSFM
38 model and found that the model is about 30% more expensive than the default ELMv0
39 with an optimal processor layout. The modular software design of VSFM not only
40 provides flexibility to configure the model for a range of problem setups, but also
41 allows building the model independently of the ELM code, thus enabling
42 straightforward testing of model's physics against other models.

Deleted: coupled

Deleted:

45 **1 Introduction**

46 Groundwater, which accounts for 30% of freshwater reserves globally, is a vital
47 human water resource. It is estimated that groundwater provides 20-30% of global
48 freshwater withdrawals (Petra, 2009; Zektser and Evertt, 2004), and that irrigation
49 accounts for ~70% of these withdrawals (Siebert et al., 2010). Climate change is
50 expected to impact the quality and quantity of groundwater in the future (Alley,
51 2001). As temporal variability of precipitation and surface water increases in the
52 future due to climate change, reliance on groundwater as a source of fresh water for
53 domestic, agriculture, and industrial use is expected to increase (Taylor et al., 2013).

54 Local environmental conditions modulate the impact of rainfall changes on
55 groundwater resources. For example, high intensity precipitation in humid areas may
56 lead to a decrease in groundwater recharge (due to higher surface runoff), while arid
57 regions are expected to see gains in groundwater storage (as infiltrating water
58 quickly travels deep into the ground before it can be lost to the atmosphere)
59 (Kundzewicz and Doli, 2009). Although global climate models predict changes in
60 precipitation over the next century (Marvel et al., 2017), few global models that
61 participated in the recent Coupled Model Inter-comparison Project (CMIP5; Taylor et
62 al. (2012)) were able to represent global groundwater dynamics accurately (e.g.
63 Swenson and Lawrence (2014))

64 Modeling studies have also investigated impacts, at watershed to global scales,
65 on future groundwater resources associated with land-use (LU) and land-cover (LC)
66 change (Dams et al., 2008) and ground water pumping (Ferguson and Maxwell, 2012;
67 Leng et al., 2015). Dams et al. (2008) predicted that LU changes would result in a small
68 mean decrease in subsurface recharge and large spatial and temporal variability in
69 groundwater depth for the Kleine Nete basin in Belgium. Ferguson and Maxwell
70 (2012) concluded that groundwater-fed irrigation impacts on water exchanges with
71 the atmosphere and groundwater resources can be comparable to those from a 2.5 °C
72 increase in air temperature for the Little Washita basin in Oklahoma, USA. By
73 performing global simulations of climate change scenarios using CLM4, Leng et al.
74 (2015) concluded that the water source (i.e., surface or groundwater) used for

75 irrigation depletes the corresponding water source while increasing the storage of
76 the other water source. Recently, Leng et al. (2017) showed that irrigation method
77 (drip, sprinkler, or flood) has impacts on water balances and water use efficiency in
78 global simulations.

79 Groundwater models are critical for developing understanding of
80 groundwater systems and predicting impacts of climate (Green et al., 2011). Kollet
81 and Maxwell (2008) identified critical zones, i.e., regions within the watershed with
82 water table depths between 1 – 5 m, where the influence of groundwater dynamics
83 was largest on surface energy budgets. Numerical studies have demonstrated impacts
84 of groundwater dynamics on several key Earth system processes, including soil
85 moisture (Chen and Hu, 2004; Liang et al., 2003; Salvucci and Entekhabi, 1995; Yeh
86 and Eltahir, 2005), runoff generation (Levine and Salvucci, 1999; Maxwell and Miller,
87 2005; Salvucci and Entekhabi, 1995; Shen et al., 2013), surface energy budgets
88 (Alkhaier et al., 2012; Niu et al., 2017; Rihani et al., 2010; Soylyu et al., 2011), land-
89 atmosphere interactions (Anyah et al., 2008; Jiang et al., 2009; Leung et al., 2011;
90 Yuan et al., 2008), vegetation dynamics (Banks et al., 2011; Chen et al., 2010), and soil
91 biogeochemistry (Lohse et al., 2009; Pacific et al., 2011).

92 Recognizing the importance of groundwater systems on terrestrial processes,
93 groundwater models of varying complexity have been implemented in land surface
94 models (LSMs) in recent years. Groundwater models in current LSMs can be classified
95 into four categories based on their governing equations. Type-1 models assume a
96 quasi-steady state equilibrium of the soil moisture profile above the water table
97 (Hilberts et al., 2005; Koster et al., 2000; Walko et al., 2000). Type-2 models use a θ -
98 based (where θ is the water volume content) Richards equation in the unsaturated
99 zone coupled with a lumped unconfined aquifer model in the saturated zone.
100 Examples of one-dimensional Type-2 models include Liang et al. (2003), Yeh and
101 Eltahir (2005), Niu et al. (2007), and Zeng and Decker (2009). Examples of quasi
102 three-dimensional Type-2 models are York et al. (2002); Fan et al. (2007); Miguez-
103 Macho et al. (2007); and Shen et al. (2013). Type-3 models include a three-
104 dimensional representation of subsurface flow based on the variably saturated

105 Richards equation (Maxwell and Miller, 2005; Tian et al., 2012). Type-3 models
106 employ a unified treatment of hydrologic processes in the vadose and phreatic zones
107 but lump changes associated with water density and unconfined aquifer porosity into
108 a specific storage term. The fourth class (Type-4) of subsurface flow and reactive
109 transport models (e.g., PFLOTRAN (Hammond and Lichtner, 2010), TOUGH2 (Pruess
110 et al., 1999), and STOMP (White and STOMP, 2000)) combine a water equation of
111 state (EoS) and soil compressibility with the variably saturated Richards equation.
112 Type-4 models have not been routinely coupled with LSMs to address climate change
113 relevant research questions. Clark et al. (2015) summarized that most LSMs use
114 different physics formulations for representing hydrologic processes in saturated and
115 unsaturated zones. Additionally, Clark et al. (2015) identified incorporation of
116 variably saturated hydrologic flow models (i.e., Type-3 and Type-4 models) in LSMs
117 as a key opportunity for future model development that is expected to improve
118 simulation of coupled soil moisture and shallow groundwater dynamics.

119 The Energy, Exascale, Earth System Model (E3SM) is a new Earth System
120 Modeling project sponsored by the U.S. Department of Energy (DOE) (E3SM Project,
121 2018). The E3SM model started from the Community Earth System Model (CESM)
122 version 1_3_beta10 (Oleson, 2013). Specifically, the initial version (v0) of the E3SM
123 Land Model (ELM) was based off the Community Land Model's (CLM's) tag 4_5_71.
124 ELMv0 uses a Type-2 subsurface hydrology model based on Zeng and Decker (2009).
125 In this work, we developed in ELMv1 a Type-4 Variably Saturated Flow model (VSFM)
126 to provide a unified treatment of soil hydrologic processes within the unsaturated
127 and saturated zones. The VSFM formulation is based on the isothermal, single phase,
128 variably-saturated (RICHARDS) flow model within PFLOTRAN (Hammond and
129 Lichtner, 2010). While PFLOTRAN is a massively parallel, three-dimensional
130 subsurface model, the VSFM is a serial, one-dimensional model that is appropriate for
131 climate scale applications.

132 This paper is organized into several sections: (1) brief review of the ELMv0
133 subsurface hydrology model; (2) overview of the VSFM formulation integrated in
134 ELMv1; (3) application of the new model formulation to three benchmark problems;
135 (4) development of a subsurface drainage parameterization necessary to predict

136 global water table depths (WTDs) comparable to recently released observationally-
137 constrained estimates; (5) comparison of ELMv1 global simulations with the default
138 subsurface hydrology model and VSFM against multiple observations using the
139 International Land Model Benchmarking package (ILAMB; Hoffman et al. (2017));
140 and (6) a summary of major findings.

141 **2 Methods**

142 **2.1 Current Model Formulation**

143 Water flow in the unsaturated zone is often described by the θ -based Richards
144 equation:

$$\frac{\partial \theta}{\partial t} = -\nabla \cdot \mathbf{q} - Q \quad (1)$$

145 where θ [m^3 of water m^{-3} of soil] is the volumetric soil water content, t [s] is time, \mathbf{q}
146 [m s^{-1}] is the Darcy water flux, and Q [m^3 of water m^{-3} of soil s^{-1}] is a soil moisture
147 sink term. The Darcy flux, \vec{q} , is given by

$$\mathbf{q} = -K\nabla(\psi + z) \quad (2)$$

149 where K [ms^{-1}] is the hydraulic conductivity, z [m] is height above some datum in the
150 soil column and ψ [m] is the soil matric potential. The hydraulic conductivity and soil
151 matric potential are modeled as non-linear function of volumetric soil moisture
152 following Clapp and Hornberger (1978):

$$K = \theta_{ice} K_{sat} \left(\frac{\theta}{\theta_{sat}} \right)^{2B+3} \quad (3)$$

$$\psi = \psi_{sat} \left(\frac{\theta}{\theta_{sat}} \right)^{-B} \quad (4)$$

153 where K_{sat} [m s^{-1}] is saturated hydraulic conductivity, ψ_{sat} [m] is saturated soil
154 matric potential, B is a linear function of percentage clay and organic content (Oleson,
155 2013), and θ_{ice} is the ice impedance factor (Swenson et al., 2012). ELMv0 uses the

157 modified form of Richards equation of Zeng and Decker (2009) that computes Darcy
158 flux as

$$\mathbf{q} = -K\nabla(\psi + z - C) \quad (5)$$

159 where C is a constant hydraulic potential above the water table, z_v , given as

$$C = \psi_E + z = \psi_{sat} \left(\frac{\theta_E(z)}{\theta_{sat}} \right)^{-B} + z = \psi_{sat} + z_v \quad (6)$$

160 where ψ_E [m] is the equilibrium soil matric potential, z [m] is height above a
161 reference datum, θ_E [$\text{m}^3 \text{m}^{-3}$] is volumetric soil water content at equilibrium soil
162 matric potential, and z_v [m] is height of water table above a reference datum. ELMv0
163 uses a cell-centered finite volume spatial discretization and backward Euler implicit
164 time integration. By default, ELMv0's vertical discretization of a soil column yields 15
165 soil layers of exponentially varying soil thicknesses that reach a depth of 42.1 m Only
166 the first 10 soils layers (or top 3.8 m of each soil column), are hydrologically active,
167 while thermal processes are resolved for all 15 soils layers. The nonlinear Darcy flux
168 is linearized using Taylor series expansion and the resulting tridiagonal system of
169 equations is solved by LU factorization.

170 Flow in the saturated zone is modeled as an unconfined aquifer below the soil
171 column based on the work of Niu et al. (2007). Exchange of water between the soil
172 column and unconfined aquifer depends on the location of the water table. When the
173 water table is below the last hydrologically active soil layer in the column, a recharge
174 flux from the last soil layer replenishes the unconfined aquifer. A zero-flux boundary
175 condition is applied to the last hydrologically active soil layer when the water table is
176 within the soil column. The unconfined aquifer is drained by a flux computed based
177 on the SIMTOP scheme of Niu et al. (2007) with modifications to account for frozen
178 soils (Oleson, 2013).

179 **2.2 New VSFM Model Formulation**

180 In the VSFM formulation integrated in ELMv1, we use the mass conservative form of
181 the variably saturated subsurface flow equation (Farthing et al., 2003; Hammond and
182 Lichtner, 2010; Kees and Miller, 2002):

$$\frac{\partial(\phi s_w \rho)}{\partial t} = -\nabla \cdot (\rho \mathbf{q}) - Q \quad (7)$$

183 where ϕ [m³ m⁻³] is the soil porosity, s_w [-] is saturation, ρ [kg m⁻³] is water density,
 184 \mathbf{q} [m s⁻¹] is the Darcy velocity, and Q [kg m⁻³ s⁻¹] is a water sink. We restrict our model
 185 formulation to a one-dimensional system and the flow velocity is defined by Darcy's
 186 law:

$$\mathbf{q} = -\frac{kk_r}{\mu} \nabla(P + \rho g z) \quad (8)$$

187 where k [m²] is intrinsic permeability, k_r [-] is relative permeability, μ [Pa s] is
 188 viscosity of water, P [Pa] is pressure, g [m s⁻²] is the acceleration due to gravity, and
 189 z [m] is elevation above some datum in the soil column.

190 In order to close the system, a constitutive relationship is used to express
 191 saturation and relative permeability as a function of soil matric pressure. Analytic
 192 Water Retention Curves (WRCs) are used to model effective saturation (s_e)

$$s_e = \left(\frac{s_w - s_r}{1 - s_r} \right) \quad (9)$$

193 where s_w is saturation and s_r is residual saturation. We have implemented Brooks
 194 and Corey (1964) (equation 10) and van Genuchten (1980) (equation 11) WRCs:

$$s_e = \begin{cases} \left(\frac{-P_c}{P_c^0} \right)^{-\lambda} & \text{if } P_c < P_c^0 \\ 1 & \text{if } P_c \geq 0 \end{cases} \quad (10)$$

$$s_e = \begin{cases} [1 + (\alpha |P_c|)^n]^{-m} & \text{if } P_c < 0 \\ 1 & \text{if } P_c \geq 0 \end{cases} \quad (11)$$

195 where P_c [Pa] is the capillary pressure, P_c^0 [Pa] is the air entry pressure, and α [Pa⁻¹]
 196 is inverse of the air entry pressure, λ [-] is the exponent in the Brooks and Corey
 197 parameterization, and n [-] and m [-] are van Genuchten parameters. The capillary
 198 pressure is computed as $P_c = P - P_{ref}$ where P_{ref} is P_c^0 for Brooks and Corey WRC
 199 and typically the atmospheric pressure (=101,325 [Pa]) is used for van Genuchten
 200 WRC. In addition, a smooth approximation of equation (10) and (11) was developed
 201 to facilitate convergence of the nonlinear solver (Appendix A). Relative soil
 202 permeability was modeled using the Mualem (1976) formulation:

Deleted: .

$$\kappa_r(s_e) = \begin{cases} s_e^{0.5} \left[1 - \left(1 - s_e^{1/m} \right)^m \right] & \text{if } P < P_{ref} \\ 1 & \text{if } P \geq P_{ref} \end{cases} \quad (12)$$

204 where $m = 1 - 1/n_e$. Lastly, we used an EoS for water density, ρ , that is a nonlinear
 205 function of liquid pressure, P , and liquid temperature, T , given by Tanaka et al.
 206 (2001):

$$\rho(P, T) = [1 + (k_0 + k_1 T + k_2 T^2)(P - P_{ref})] a_5 \left[1 - \frac{(T + a_1)^2 (T + a_2)}{a_3 (T + a_4)} \right] \quad (13)$$

207 where

$$k_0 = 50.74 \times 10^{-11} [\text{Pa}^{-1}]$$

$$k_1 = -0.326 \times 10^{-11} [\text{Pa}^{-1}\text{C}^{-1}]$$

$$k_2 = 0.00416 \times 10^{-11} [\text{Pa}^{-1}\text{C}^2]$$

$$a_1 = -3.983035 [\text{C}]$$

$$a_2 = 301.797 [\text{C}]$$

$$a_3 = 522558.9 [\text{C}^{-2}]$$

$$a_4 = 69.34881 [\text{C}]$$

$$a_5 = 999.974950 [\text{kg m}^{-3}]$$

208 The sink of water due to transpiration from a given plant functional type (PFT)
 209 is vertically distributed over the soil column based on area and root fractions of the
 210 PFT. The top soil layer has an additional flux associated with balance of infiltration
 211 and soil evaporation. The subsurface drainage flux is applied proportionally to all soil
 212 layers below the water table. Details on the computation of water sinks are given in
 213 Oleson (2013) Unlike the default subsurface hydrology model, the VSFM is applied
 214 over the full soil depth (in the default model, 15 soil layers). The VSFM model replaces
 215 both the θ -based Richards equation and the unconfined aquifer of the default model
 216 and uses a zero-flux lower boundary condition. In the VSFM model, water table depth
 217 is diagnosed based on the vertical soil liquid pressure profile. Like the default model,
 218 drainage flux is computed based on the modified SIMTOP approach and is vertically
 219 distributed over the soil layers below the water table.

220 **2.2.1 Discrete Equations**

221 We use a cell-centered finite volume discretization to decompose the spatial
 222 domain, Ω , into N non-overlapping control volumes, Ω_n , such that $\Omega = \cup_{n=1}^N \Omega_i$ and Γ_n
 223 represents the boundary of the n -th control volume. Applying a finite volume integral
 224 to equation (7) and the divergence theorem yields

$$\frac{\partial}{\partial t} \int_{\Omega_n} (\phi S_w \rho) dV = - \int_{\Gamma_n} (\rho \mathbf{q}) \cdot d\mathbf{A} - \int_{\Omega_n} Q dV \quad (14)$$

225 The discretized form of the left hand side term and first term on the right hand side
 226 of equation (14) are approximated as:

227

$$\frac{\partial}{\partial t} \int_{\Omega_n} (\phi S_w \rho) dV \approx \left(\frac{d}{dt} (\phi S_w \rho) \right) V_n \quad (15)$$

$$\int_{\Gamma_n} (\rho \mathbf{q}) \cdot d\mathbf{A} \approx \sum_{n'} (\rho \mathbf{q})_{nn'} \cdot \mathbf{A}_{nn'} \quad (16)$$

228 where $\mathbf{A}_{nn'}$ [m^2] is the common face area between the n -th and n' -th control volumes.
 229 After substituting equations (15) and (16) in equation (14), the resulting ordinary
 230 differential equation for the variably saturated flow model is

$$\left(\frac{d}{dt} (\phi S_w \rho) \right) V_n = - \sum_{n'} (\rho \mathbf{q})_{nn'} \cdot \mathbf{A}_{nn'} - Q_n V_n \quad (17)$$

231 We perform temporal integration of equation (17) using the backward-Euler scheme:

$$\left(\frac{(\phi S_w \rho)_n^{t+1} - (\phi S_w \rho)_n^t}{\Delta t} \right) V_n = - \sum_{n'} (\rho \mathbf{q})_{nn'}^{t+1} \cdot \mathbf{A}_{nn'} - Q_n^{t+1} V_n \quad (18)$$

232 Rearranging terms of equation (18) results in a nonlinear equation for the unknown
 233 pressure at timestep $t + 1$ as

$$\left(\frac{(\phi S_w \rho)_n^{t+1} - (\phi S_w \rho)_n^t}{\Delta t} \right) V_n + \sum_{n'} (\rho \mathbf{q})_{nn'}^{t+1} \cdot \mathbf{A}_{nn'} + Q_n^{t+1} V_n = 0 \quad (19)$$

234 In this work, we find the solution to the nonlinear system of equations given by
 235 equation (19) using Newton's method via the Scalable Nonlinear Equations Solver
 236 (SNES) within the Portable, Extensible Toolkit for Scientific Computing (PETSc)

Deleted: nonlinear

238 library (Balay et al., 2016). PETSc provides a suite of data structures and routines for
239 the scalable solution of partial differential equations. VSFM uses the composable data
240 management (DMComposite) provided by PETSc (Brown et al., 2012), which enables
241 the potential future application of the model to solve tightly coupled multi-
242 component, multi-physics processes as discussed in section 3.4. A Smooth
243 approximation of the Brooks and Corey (1964) (SBC) water retention curve was
244 developed to facilitate faster convergence of the nonlinear solver (Appendix A).
245 ELMv0 code for subsurface hydrologic processes only supports two vertical mesh
246 configurations and a single set of boundary and source-sink conditions. ~~The~~
247 monolithic ELMv0 code does not allow for building of code for individual process
248 representations independent of ELMv0 code, thus precluding easy testing of the
249 model against analytical solutions or simulation results from other models. The
250 modular software design of VSFM overcomes ELMv0's software limitation by
251 allowing VSFM code to be built independently of the ELM code. This flexibility of
252 VSFM's build system allows for testing of the VSFM physics in isolation without any
253 influence from the rest of ELM's physics formulations. Additionally, VSFM can be
254 easily configured for a wide range of benchmark problems with different spatial grid
255 resolutions, material properties, boundary conditions, and source-sink forcings.

Deleted: Moreover, the

Deleted: testing

256 **2.3 VSFM single-column evaluation**

257 We tested the VSFM with three idealized 1-dimensional test problems. First, the
258 widely studied problem for 1D Richards equation of infiltration in dry soil by Celia et
259 al. (1990) was used. The problem setup consists of a 1.0 m long soil column with a
260 uniform initial pressure of -10.0 m (= 3535.5 Pa). Time invariant boundary
261 conditions applied at the top and bottom of soil column are -0.75 m (= 93989.1 Pa)
262 and -10.0 m (= 3535.5 Pa), respectively. The soil properties for this test are given in
263 Table 1. A vertical discretization of 0.01 m is used in this simulation.

264 Second, we simulated transient one-dimensional vertical infiltration in a two-
265 layered soil system as described in Srivastava and Yeh (1991). The domain consisted
266 of a 2 m tall soil column divided equally in two soil types. Except for soil intrinsic
267 permeability, all other soil properties of the two soil types are the same. The bottom

270 soil is 10 times less permeable than the top (Table1). Unlike Srivastava and Yeh
271 (1991), who used exponential functions of soil liquid pressure to compute hydraulic
272 conductivity and soil saturation, we used Mualem (1976) and van Genuchten (1980)
273 constitutive relationships. Since our choice of constitutive relationships for this setup
274 resulted in absence of an analytical solution, we compared VSFM simulations against
275 PFLOTRAN results. The domain was discretized in 200 control volumes of equal soil
276 thickness. Two scenarios, wetting and drying, were modeled to test the robustness of
277 the VSFM solver robustness. Initial conditions for each scenario included a time
278 invariant boundary condition of 0 m ($= 1.01325 \times 10^5$ Pa) for the lowest control
279 volume and a constant flux of 0.9 cm hr^{-1} and 0.1 cm hr^{-1} at the soil surface for wetting
280 and drying scenarios, respectively.

281 Third, we compare VSFM and PFLOTRAN predictions for soil under variably
282 saturated conditions. The 1-dimensional 1 m deep soil column was discretized in 100
283 equal thickness control volumes. A hydrostatic initial condition was applied such that
284 water table is 0.5 m below the soil surface. A time invariant flux of $2.5 \times 10^{-5} \text{ m s}^{-1}$ is
285 applied at the surface, while the lowest control volume has a boundary condition
286 corresponding to the initial pressure value at the lowest soil layer. The soil properties
287 used in this test are the same as those used in the first evaluation.

288 **2.4 Global Simulations and groundwater depth analysis**

289 We performed global simulations with ELMv1-VSFM at a spatial resolution of
290 1.9° (latitude) \times 2.5° (longitude) with a 30 [min] time-step for 200 years, including a
291 180 year spinup and the last 20 years for analysis. The simulations were driven by
292 CRUNCEP meteorological forcing from 1991-2010 (Piao et al., 2012) and configured
293 to use prescribed satellite phenology.

294 For evaluation and calibration, we used the Fan et al. (2013) global ~ 1 km
295 horizontal resolution WTD dataset (hereafter F2013 dataset), which is based on a
296 combination of observations and hydrologic modeling. We aggregated the dataset to
297 the ELMv1-VSFM spatial resolution. ELM-VSFM's default vertical soil discretization
298 uses 15 soil layers to a depth of ~ 42 m, with an exponentially varying soil thickness.
299 However, $\sim 13\%$ of F2013 land gridcells have a water table deeper than 42 m. We

300 therefore modified ELMv1-VSFM to extend the soil column to a depth of 150 m with
301 59 soil layers; the first nine soil layer thicknesses were the same as described in
302 Oleson (2013) and the remaining layers (10-59) were set to a thickness of 3 m.

303 2.5 Estimation of the subsurface drainage parameterization

304 In the VSFM formulation, the dominant control on long-term GW depth is the
305 subsurface drainage flux, q_d [$\text{kg m}^{-2} \text{s}^{-1}$], which is calculated based on water table
306 depth, z_v [m], (Niu et al. (2005)):

$$q_d = q_{d,max} \exp(-f_d z_v) \quad (20)$$

307 where $q_{d,max}$ [$\text{kg m}^{-2} \text{s}^{-1}$] is the maximum drainage flux that depends on gridcell slope
308 and f_d [m^{-1}] is an empirically-derived parameter. The subsurface drainage flux
309 formulation of Niu et al. (2005) is similar to the TOPMODEL formulation (Beven and
310 Kirkby, 1979) and assumes the water table is parallel to the soil surface. While
311 Sivapalan et al. (1987) derived $q_{d,max}$ as a function of lateral hydraulic anisotropy,
312 hydraulic conductivity, topographic index, and decay factor controlling vertical
313 saturated hydraulic conductivity, Niu et al. (2005) defined $q_{d,max}$ as a single
314 calibration parameter. ELMv0 uses $f_d = 2.5 \text{ m}^{-1}$ as a global constant and estimates
315 maximum drainage flux when WTD is at the surface as $q_{d,max} = 10 \sin(\beta) \text{ kg m}^{-2} \text{ s}^{-1}$,
316 where β [radians] is mean grid cell topographic slope. Of the two parameters, f_d and
317 $q_{d,max}$, available for model calibration, we choose to calibrate f_d because the
318 uncertainty analysis by Hou et al. (2012) identified it as the most significant
319 hydrologic parameter in CLM4. To improve on the f_d parameter values, we
320 performed an ensemble of global simulations with f_d values of 0.1, 0.2, 0.5, 1.0, 2.5,
321 5.0, 10.0, and 20 m^{-1} . Each ensemble simulation was run for 200 years to ensure an
322 equilibrium solution, and the last 20 years were used for analysis. A non-linear
323 functional relationship between f_d and WTD was developed for each gridcell and
324 then the F2013 dataset was used to estimate an optimal f_d for each gridcell.

325 2.6 Global ELM-VSFM evaluation

326 With the optimal f_d values, we ran a ELM-VSFM simulation using the protocol
327 described above. We then used the International Land Model Benchmarking package

Deleted: $\sin(\beta)$

329 (ILAMB) to evaluate the ELMv1-VSFM predictions of surface energy budget, total
330 water storage anomalies (TWSA), and river discharge (Collier et al., 2018; Hoffman et
331 al., 2017). ILAMB evaluates model prediction bias, RMSE, and seasonal and diurnal
332 phasing against multiple observations of energy, water, and carbon cycles at in-situ,
333 regional, and global scales. Since ELM-VSFM simulations in this study did not include
334 an active carbon cycle, we used the following ILAMB benchmarks for water and
335 energy cycles: (i) latent and surface energy fluxes using site-level measurements from
336 FLUXNET (Lasslop et al., 2010) and globally from FLUXNET-MTE (Jung et al., 2009));
337 (ii) terrestrial water storage anomaly (TWSA) from the Gravity Recovery And Climate
338 Experiment (GRACE) observations (Kim et al., 2009); and (iii) stream flow for the 50
339 largest global river basins (Dai and Trenberth, 2002). We applied ILAMB benchmarks
340 for ELMv1-VSFM simulations with default and calibrated f_d to ensure improvements
341 in WTD predictions did not degrade model skill for other processes.

342 **3 Results and discussion**

343 **3.1 VSFM single-column evaluation**

344 For the 1D Richards equation infiltration in dry soil comparison, we evaluated
345 the solutions at 24-hr against those published by Celia et al. (1990) (Figure 1). The
346 VSFM solver accurately represented the sharp wetting front over time, where soil
347 hydraulic properties change dramatically due to non-linearity in the soil water
348 retention curve.

Deleted: Figure 1

349 For the model evaluation of infiltration and drying in layered soil, the results of
350 the VSFM and PFLOTRAN are essentially identical. In both models and scenarios, the
351 higher permeability top soil responds rapidly to changes in the top boundary
352 condition and the wetting and drying fronts progressively travel through the less
353 permeable soil layer until soil liquid pressure in the entire column reaches a new
354 steady state by about 100 h (Figure 2).

Deleted: Figure 2

355 We also evaluated the VSFM predicted water table dynamics against PFLOTRAN
356 predictions from an initial condition of saturated soil below 0.5 m depth. The
357 simulated water table rises to 0.3 m depth by 1 day and reaches the surface by 2 days,

360 and the VSFM and PFLOTRAN predictions are essentially identical [Figure 3](#), [Soil](#)
361 [properties, spatial discretization, and timestep used for the three single-column](#)
362 [problems are summarized in Table 1](#). These three evaluation simulations demonstrate
363 the VSFM accurately represents soil moisture dynamics under conditions relevant to
364 ESM-scale prediction.

Deleted: Figure 3

365 3.2 Subsurface drainage parameterization estimation

366 The simulated nonlinear WTD- f_d relationship is a result of the subsurface
367 drainage parameterization flux given by equation (20) ([Figure 4\(a\)](#) and (b)). For
368 $0.1 \leq f_d \leq 1$, the slope of the WTD- f_d relationship for all gridcells is log-log linear
369 with a slope of -1.0 ± 0.1 . The log-log linear relationship breaks down for $f_d > 1$,
370 where the drainage flux becomes much smaller than infiltration and
371 evapotranspiration ([Figure 4\(c\)](#) and (d)). Thus, at larger f_d , the steady state z_v
372 becomes independent of f_d and is determined by the balance of infiltration and
373 evapotranspiration.

Deleted: Figure 4

374 For 79% of the global gridcells, the ensemble range of simulated WTD spanned
375 the F2013 dataset. The optimal value of f_d for each of these gridcells was obtained by
376 linear interpolation in the log-log space (e.g., [Figure 4\(a\)](#)). For the remaining 21% of
377 gridcells where the shallowest simulated WTD across the range of f_d was deeper than
378 that in the F2013 dataset, the optimal f_d value was chosen as the one that resulted in
379 the lowest absolute WTD error (e.g., [Figure 4\(b\)](#)). At large f_d values, the drainage flux
380 has negligible effects on WTD, yet simulated WTD is not sufficiently shallow to match
381 the F2013 observations, which indicates that either evapotranspiration is too large
382 or infiltration is too small. There was no difference in the mean percentage of sand
383 and clay content between grids cells with and without an optimal f_d value. The
384 optimal f_d has a global average of $1.60 \text{ m}^{-1} \pm 2.68 \text{ m}^{-1}$ and 72% of global gridcells have
385 an optimal f_d value lower than the global average ([Figure 5](#)).

Deleted: Figure 4

Deleted: Figure 4

Deleted: Figure 4

Deleted: Figure 5

386 3.3 Global simulation evaluation

387 The ELMv1-VSFM predictions are much closer to the F2013 dataset ([Figure 6a](#))
388 using optimal globally-distributed f_d values ([Figure 6c](#)) compared to the default f_d

395 value (Figure 6b). The significant reduction in WTD bias (model – observation) is
396 mostly due to improvement in the model's ability to accurately predict deep WTD
397 using optimal f_d values. In the simulation using optimal globally-distributed f_d
398 values, all gridcells with WTD bias > 3.7 m were those for which an optimal f_d was
399 not found. The mean global bias, RMSE, and R^2 values improved in the new ELMv1-
400 VSFM compared to the default model (Table 2). The 79% of global grid cells for which
401 an optimal f_d value was estimated had significantly better water table prediction
402 with a bias, RMSE, and R^2 of -0.04 m, 0.67 m, and 0.99, respectively, as compared to
403 the remaining 21% of global gridcells that had a bias, RMSE, and R^2 of -9.82 m, 18.08
404 m, and 0.31, respectively. The simulated annual WTD range, which we define to be
405 the difference between maximum and minimum WTD in a year, has a spatial mean
406 and standard deviation of 0.32 m and 0.58 m, respectively, using optimal f_d values
407 (Figure 7, (a)). The annual WTD range decreased by 0.24 m for the 79% of the grid
408 cells for which an optimal f_d value was estimated (Figure 7, (b)).

Deleted: Table 1).

Deleted: Figure 7

Deleted: Figure 7

409 Globally-averaged WTD in ELMv1-VSFM simulations with default f_d and
410 optimal f_d values were 10.5 m and 20.1 m, respectively. Accurate prediction of deep
411 WTD in the simulation with optimal f_d caused very small differences in near-surface
412 soil moisture (Figure 8). The 79% of grid cells with an optimal f_d value had deeper
413 globally-averaged WTDs than when using the default f_d value (24.3 m vs. 8.6 m). For
414 these 79% of grid cells, the WTD was originally deep enough to not impact near-
415 surface conditions (Kollet and Maxwell, 2008); therefore, further lowering of WTD
416 led to negligible changes in near-surface hydrological conditions.

Deleted: Figure 8

417 The International Land Model Benchmarking (ILAMB) package (Hoffman et al.,
418 2017) provides a comprehensive evaluation of predictions of carbon cycle states and
419 fluxes, hydrology, surface energy budgets, and functional relationships by
420 comparison to a wide range of observations. We used ILAMB to evaluate the
421 hydrologic and surface energy budget predictions from the new ELMv1-VSFM model
422 (Table 3). Optimal f_d values had inconsequential impacts on simulated surface
423 energy fluxes at site-level and global scales. Optimal f_d values led to improvement in
424 prediction of deep WTD (with a mean value of 24.3 m) for grid cells that had an
425 average WTD of 8.7 m in the simulation using default f_d values. Thus, negligible

Deleted: Table 3

431 differences in surface energy fluxes between the two simulations are consistent with
432 the findings of Kollet and Maxwell (2008), who identified decoupling of groundwater
433 dynamics and surface processes at a WTD of ~10 m. There were slight changes in bias
434 and RMSE for predicted TWSA, but the ILAMB score remained unchanged. The TWSA
435 amplitude is lower for the simulation with optimal f_d values, consistent with the
436 associated decrease in annual WTD range. ELM's skill in simulating runoff for the 50
437 largest global watersheds remained unchanged. [Two additional 10-years long
438 simulations were performed to investigate the sensitivity of VSFM simulated WTD to
439 spatial and temporal discretization. Results show that simulated WTD is insensitive
440 to temporal discretization, and has small sensitivity to vertical spatial resolution. See
441 supplementary material for details regarding setup and analysis of results from the
442 two additional simulations.](#)

443 Finally, we evaluated the computational costs of implementing VSFM in ELM
444 and compared them to the default model. We performed 5-year long simulations for
445 default and VSFM using 96, 192, 384, 768, and 1536 cores on the Edison
446 supercomputer at the National Energy Research Scientific Computing Center. Using
447 an optimal processor layout, we found that ELMv1-VSFM is ~30% more expensive
448 than the default ELMv1 model. [\(Supplementary material Fig S 1\)](#). We note that the
449 relative computational cost of the land model in a fully coupled global model
450 simulation is generally very low. Dennis et al. (2012) reported computational cost of
451 the land model to be less than 1% in ultra-high-resolution CESM simulations. We
452 therefore believe that the additional benefits associated with the VSFM formulation
453 are well justified by this modest increase in computational cost. In particular, VSFM
454 allows a greater variety of mesh configurations and boundary conditions, and can
455 accurately simulate WTD for the ~13% of global grid cells that have a water table
456 deeper than 42 [m] (Fan et al. (2013)).

457 3.4 Caveats and Future Work

458 The significant improvement in WTD prediction using optimal f_d values
459 demonstrates VSFM's capabilities to model hydrologic processes using a unified
460 physics formulation for unsaturated-saturated zones. However, several caveats

Deleted: .

462 remain due to uncertainties in model structure, model parameterizations, and climate
463 forcing data.

464 In this study, we assumed a spatially homogeneous depth to bedrock (DTB) of
465 150 m. Recently, Brunke et al. (2016) incorporated a global ~1 km dataset of soil
466 thickness and sedimentary deposits (Pelletier et al., 2016) in CLM4.5 to study the
467 impacts of soil thickness spatial heterogeneity on simulated hydrological and thermal
468 processes. While inclusion of heterogeneous DTB in CLM4.5 added more realism to
469 the simulation setup, no significant changes in simulated hydrologic and energy
470 fluxes were reported by Brunke et al. (2016). Presently, work is ongoing in the E3SM
471 project to include variable DTB within ELM and future simulations will examine the
472 impact of those changes on VSFM's prediction of WTD. Our use of the 'satellite
473 phenology' mode, which prescribes transient LAI profiles for each plant functional
474 type in the gridcell, ignored the likely influence of water cycle dynamics and nutrient
475 constraints on the C cycle (Ghimire et al., 2016; Zhu et al., 2016). Estimation of soil
476 hydraulic properties based on soil texture data is critical for accurate LSM predictions
477 (Gutmann and Small, 2005) and this study does not account for uncertainty in soil
478 hydraulic properties.

479 Lateral water redistribution impacts soil moisture dynamics (Bernhardt et al.,
480 2012), biogeochemical processes in the root zone (Grant et al., 2015), distribution of
481 vegetation structure (Hwang et al., 2012), and land-atmosphere interactions (Chen
482 and Kumar, 2001; Rihani et al., 2010). The ELMv1-VSFM developed in this study does
483 not include lateral water redistribution between soil columns and only simulates
484 vertical water transport. Lateral subsurface processes can be included in LSMs via a
485 range of numerical discretization approaches of varying complexity, e.g., adding
486 lateral water as source/sink terms in the 1D model, implementing an operator split
487 approach to solve vertical and lateral processes in a non-iterative approach (Ji et al.,
488 2017), or solving a fully coupled 3D model (Bisht et al., 2017; Bisht et al., 2018; Kollet
489 and Maxwell, 2008). Additionally, lateral transport of water can be implemented in
490 LSMs at a subgrid level (Milly et al., 2014) or grid cell level (Miguez-Macho et al.,
491 2007). The current implementation of VSFM is such that each processor solves the
492 variably saturated Richards equation for all independent soil columns as one single

493 problem. Thus, extension of VSFM to solve the tightly coupled 3D Richards equation
494 on each processor locally while accounting for lateral transport of water within grid
495 cells and among grid cells is straightforward. The current VSFM implementation can
496 also be easily extended to account for subsurface transport of water among grid cells
497 that are distributed across multiple processors by modeling lateral flow as
498 source/sink terms in the 1D model. Tradeoffs between approaches to represent
499 lateral processes and computational costs need to be carefully studied before
500 developing quasi or fully three-dimensional land surface models (Clark et al., 2015).

501 Transport of water across multiple components of the Soil Plant Atmosphere
502 Continuum (SPAC) has been identified as a critical process in understanding the
503 impact of climate warming on the global carbon cycle (McDowell and Allen, 2015).
504 Several SPAC models have been developed by the ecohydrology community and
505 applied to study site-level processes (Amenu and Kumar, 2008; Bohrer et al., 2005;
506 Manoli et al., 2014; Sperry et al., 1998), yet implementation of SPAC models in global
507 LSMs is limited (Clark et al., 2015). Similarly, current generation LSMs routinely
508 ignore advective heat transport within the subsurface, which has been shown to be
509 important in high-latitude environments by multiple field and modeling studies
510 (Bense et al., 2012; Frampton et al., 2011; Grant et al., 2017; Kane et al., 2001). The
511 use of PETSc's DMComposite in VSFM provides flexibility for solving a tightly coupled
512 multi-component problem (e.g., transport of water through the soil-plant continuum)
513 and multi-physics problem (e.g., fully coupled conservation of mass and energy
514 equations in the subsurface). DMComposite allows for an easy assembly of a tightly
515 coupled multi-physics problem from individual physics formulations (Brown et al.,
516 2012).

517 **4 Summary and Conclusion**

518 Starting from the climate-scale land model ELMv0, we incorporated a unified
519 physics formulation to represent soil moisture and groundwater dynamics that are
520 solved using PETSc. Application of VSFM to three benchmarks problems
521 demonstrated its robustness to simulated subsurface hydrologic processes in

522 coupled unsaturated and saturated zones. Ensemble global simulations at $1.9^0 \times 2.5^0$
 523 were performed for 200 years to obtain spatially heterogeneous estimates of the
 524 subsurface drainage parameter, f_d , that minimized mismatches between predicted
 525 and observed WTDs. In order to simulate the deepest water table reported in the Fan
 526 et al. (2013) dataset, we used 59 vertical soil layers that reached a depth of 150 m.

527 An optimal f_d was obtained for 79% of the grids cells in the domain. For the
 528 remaining 21% of grid cells, simulated WTD always remained deeper than observed.
 529 Calibration of f_d significantly improved global WTD prediction by reducing bias and
 530 RMSE and increasing R^2 . Grids without an optimal f_d were the largest contributor of
 531 error in WTD prediction. ILAMB benchmarks on simulations with default and
 532 optimal f_d showed negligible changes to surface energy fluxes, TWSA, and runoff.
 533 ILAMB metrics ensured that model skill was not adversely impacted for all other
 534 processes when optimal f_d values were used to improve WTD prediction.

535

536 5 Appendix

537 5.1 Smooth approximation of Brooks-Corey water retention curve

538 The Brooks and Corey (1964) water retention curve of equation (10) has a
 539 discontinuous derivative at $P = P_c^0$. Figure A 1, illustrates an example. To improve
 540 convergence of the nonlinear solver at small capillary pressures, the smoothed
 541 Brooks-Corey function introduces a cubic polynomial, $B(P_c)$, in the neighborhood of
 542 P_c^0 .

$$s_e = \begin{cases} (-\alpha P_c)^{-\lambda} & \text{if } P_c \leq P_u \\ B(P_c) & \text{if } P_u < P_c < P_s \\ 1 & \text{if } P_s \leq P_c \end{cases} \quad (21)$$

543 where the breakpoints P_u and P_s satisfy $P_u < P_c^0 < P_s \leq 0$. The smoothing
 544 polynomial

$$B(P_c) = b_0 + b_1(P_c - P_s) + b_2(P_c - P_s)^2 + b_3(P_c - P_s)^3 \quad (22)$$

545 introduces four more parameters, whose values follow from continuity. In particular
 546 matching the saturated region requires $B(P_s) = b_0 = 1$, and a continuous derivative

Formatted: Font: Cambria

Deleted: 10

Deleted: Figure A 1

Formatted: Font: Cambria

549 at $P_c = P_s$ requires $B'(P_s) = b_1 = 0$. Similarly, matching the value and derivative at
 550 $P_c = P_u$ requires

$$b_2 = \frac{-1}{\Delta^2} \left[3 - (\alpha P_u)^{-\lambda} \left(3 + \frac{\lambda \Delta}{P_u} \right) \right] \quad (23)$$

$$b_3 = \frac{-1}{\Delta^3} \left[2 - (\alpha P_u)^{-\lambda} \left(2 + \frac{\lambda \Delta}{P_u} \right) \right] \quad (24)$$

551 where $\Delta = P_u - P_s$. Note $P_u \leq \Delta < 0$.

552 In practice, setting P_u too close to P_c^0 can produce an unwanted local maximum
 553 in the cubic smoothing regime, resulting in $s_e > 1$. Avoiding this condition requires
 554 that $B(P_c)$ increase monotonically from $P_c = P_u$, where $B'(P_c) > 0$, to $P_c = P_s$, where
 555 $B'(P_c) = 0$. Thus a satisfactory pair of breakpoints ensures

$$B'(P_c) = [P_c - P_s][2b_2 + 3b_3(P_c - P_s)] > 0 \quad (25)$$

556 throughout $P_u \leq P_c < P_s$.

557 Let P_c^* denote a local extremum of B , so that $B'(P_c^*) = 0$. If $P_c^* \neq P_s$, it follows
 558 $P_c^* - P_s = -2b_2/(3b_3)$. Rewriting equation 22, $B'(P_c) = (P_c - P_s)3b_3(P_c - P_c^*)$ shows
 559 that $B'(P_c^*) > 0$ requires either: (1) $b_3 < 0$ and $P_c^* < P_u$; or (2) $b_3 > 0$ and $P_c^* > P_u$.
 560 The first possibility places P_c^* outside the cubic smoothing regime, and so does not
 561 constrain the choice of P_u or P_s . The second possibility allows an unwanted local
 562 extremum at $P_u < P_c^* < P_s$. In this case, $b_3 > 0$ implies $b_2 < 0$ (since $P_c^* < P_s \leq 0$).
 563 Then since $B''(P_c^*) = -2b_2$, the local extremum is a maximum, resulting in $s_e(P_c^*) >$
 564 1.

565 Given a breakpoint P_s , one strategy for choosing P_u is to guess a value, then
 566 check whether the resulting b_2 and b_3 produces $P_u < P_c^* < P_s$. If so, P_u should be
 567 made more negative. An alternative strategy is to choose P_u in order the guarantee
 568 acceptable values for b_2 and b_3 . One convenient choice forces $b_2 = 0$. Another picks
 569 P_u in order to force $b_3 = 0$. Both of these reductions: (1) ensure $B(P_c)$ has a positive
 570 slope throughout the smoothing interval; (2) slightly reduce the computation cost of
 571 finding $s_e(P_c)$ for P_c on the smoothing interval; and (3) significantly reduce the
 572 computational cost of inverting the model, in order to find P_c as a function of s_e .

573 As shown in [Figure A 1](#), the two reductions differ mainly in that setting $b_2 = 0$
 574 seems to produce narrower smoothing regions (probably due to the fact that this

Deleted: Figure A 1

576 choice gives zero curvature at $P_c = P_s$, while $b_3 = 0$ yields a negative second
 577 derivative there). However, we have not verified this observation analytically.

578 Both reductions require solving a nonlinear expression either equation (23) or
 579 (24), for P_u . While details are beyond the scope of this paper, we note that we have
 580 used a bracketed Newton-Raphson's method. The search switches to bisection when
 581 Newton-Raphson would jump outside the bounds established by previous iterations,
 582 and by the requirement $P_u < P_c^0$. In any event, since the result of this calculation may
 583 be cached for use throughout the simulation, it need not be particularly efficient.

584 5.2 Residual equation of VSFM formulation

585 The residual equation for the VSFM formulation at $t + 1$ time level for n -th control
 586 volume is given by

$$R_n^{t+1} \equiv \left(\frac{(\phi s_w \rho)_n^{t+1} - (\phi s_w \rho)_n^t}{\Delta t} \right) V_n + \sum_{n'} (\rho \mathbf{q})_{nn'}^{t+1} \cdot \mathbf{A}_{nn'} + Q_n^{t+1} V_n = 0 \quad (26)$$

587 where ϕ [$\text{mm}^3 \text{mm}^{-3}$] is the soil porosity, s_w [-] is saturation, ρ [kg m^{-3}] is water
 588 density, $\vec{q}_{nn'}$ [m s^{-1}] is the Darcy flow velocity between n -th and n' -th control
 589 volumes, $A_{nn'}$ [m^2] is the interface face area between n -th and n' -th control
 590 volumes Q [$\text{kg m}^{-3} \text{s}^{-1}$] is a sink of water. The Darcy velocity is computed as

$$\mathbf{q}_{nn'} = - \left(\frac{\kappa \kappa_r}{\mu} \right)_{nn'} \left[\frac{P_{n'} - P_n - \rho_{nn'} (\mathbf{g} \cdot \mathbf{d}_{nn'})}{d_n + d_{n'}} \right] \mathbf{n}_{nn'} \quad (27)$$

591 where κ [m^2] is intrinsic permeability, κ_r [-] is relative permeability, μ [Pa s] is
 592 viscosity of water, P [Pa] is pressure, \mathbf{g} [m s^{-2}] is the acceleration due to gravity,
 593 d_n [m] and $d_{n'}$ [m] is distance between centroid of n -th and n' -th control volume to
 594 the common interface between the two control volumes, $\mathbf{d}_{nn'}$ is a distance vector
 595 joining centroid of n -th and n' -th control volume, and $\mathbf{n}_{nn'}$ is a unit normal vector
 596 joining centroid of n -th and n' -th control volume.

597 The density at the interface of control volume, $\rho_{nn'}$, is computed as inverse
 598 distance weighted average by

$$\rho_{nn'} = \omega_{n'} \rho_n + \omega_n \rho_{n'} \quad (28)$$

599 where ω_n and $\omega_{n'}$ are given by

$$\omega_n = \frac{d_n}{d_n + d_{n'}} = (1 - \omega_{n'}) \quad (29)$$

600 The first term on the RHS of equation 27 is computed as the product of distance
 601 weighted harmonic average of intrinsic permeability, $k_{nn'}$, and upwinding of
 602 k_r/μ ($= \lambda$) as

$$\left(\frac{k k_r}{\mu}\right)_{nn'} = k_{nn'} \left(\frac{k_r}{\mu}\right)_{nn'} = \left[\frac{k_n k_{n'} (d_n + d_{n'})}{k_n d_{n'} + k_{n'} d_n}\right] \lambda_{nn'} \quad (30)$$

603 where

$$\lambda_{nn'} = \begin{cases} (k_r/\mu)_n & \text{if } \vec{q}_{nn'} > 0 \\ (k_r/\mu)_{n'} & \text{otherwise} \end{cases} \quad (31)$$

604 By substituting equation 28, 29 and 30 in equation 27, we obtain

$$\mathbf{q}_{nn'} = - \left[\frac{k_n k_{n'}}{k_n d_{n'} + k_{n'} d_n} \right] \lambda_{nn'} [P_{n'} - P_n - \rho_{nn'}(\mathbf{g} \cdot \mathbf{d}_{nn'})] \mathbf{n}_{nn'} \quad (32)$$

605

606 5.3 Jacobian equation of VSFM formulation

607 The discretized equations of VSFM leads to a system of nonlinear equations given by
 608 $\mathbf{R}^{t+1}(\mathbf{P}^{t+1}) = \mathbf{0}$, which are solved using Newton's method using the Portable,
 609 Extensible Toolkit for Scientific Computing (PETSc) library. The algorithm of
 610 Newton's method requires solution of the following linear problem

$$\mathbf{J}^{t+1,k}(\mathbf{P}^{t+1,k}) \Delta \mathbf{P}^{t+1,k} = -\mathbf{R}^{t+1,k}(\mathbf{P}^{t+1,k}) \quad (33)$$

611 where $\mathbf{J}^{t+1,k}(\mathbf{P}^{t+1,k})$ is the Jacobian matrix. In VSFM, the Jacobian matrix is
 612 computed analytically. The contribution to the diagonal and off-diagonal entry of the
 613 Jacobian matrix from n -th residual equations are given by

$$J_{nn} = \frac{\partial R_n}{\partial P_n} = \left(\frac{V_n}{\Delta t}\right) \frac{\partial(\rho \phi s_w)}{\partial P_n} + \sum_{n'} \frac{\partial(\rho \mathbf{q})_{nn'}}{\partial P_n} \mathbf{A}_{nn'} + \frac{\partial Q_n^{t+1}}{\partial P_n} V_n \quad (34)$$

$$J_{nn'} = \frac{\partial R_n}{\partial P_{n'}} = \sum_{n'} \frac{\partial(\rho \mathbf{q})_{nn'}}{\partial P_{n'}} \mathbf{A}_{nn'} + \frac{\partial Q_n^{t+1}}{\partial P_{n'}} V_n \quad (35)$$

614 The derivative of the accumulation term in J_{nn} is computed as

$$\frac{\partial(\rho \phi s_w)}{\partial P_n} = \phi s_w \frac{\partial \rho}{\partial P_n} + \rho s_w \frac{\partial \phi}{\partial P_n} + \rho \phi \frac{\partial s_w}{\partial P_n} \quad (36)$$

615 The derivative of flux between n -th and n' -th control volume with respect to
 616 pressure of each control volume is given as

$$\frac{\partial(\rho\mathbf{q})_{nn'}}{\partial P_n} = \rho_{nn'} \frac{\partial \mathbf{q}_{nn'}}{\partial P_n} + \mathbf{q}_{nn'} \omega_n \frac{\partial \rho_n}{\partial P_n} \quad (37)$$

617

$$\frac{\partial(\rho\mathbf{q})_{nn'}}{\partial P_{n'}} = \rho_{nn'} \frac{\partial \mathbf{q}_{nn'}}{\partial P_{n'}} + \mathbf{q}_{nn'} \omega_{n'} \frac{\partial \rho_{n'}}{\partial P_{n'}} \quad (38)$$

618 Lastly, the derivative of Darcy velocity between n -th and n' -th control volume with
 619 respect to pressure of each control volume is given as

$$\frac{\partial \mathbf{q}_{nn'}}{\partial P_n} = \left[\frac{k_n k_{n'}}{k_n d_{n'} + k_{n'} d_n} \right] \lambda_{nn'} \left[1 + \omega_n (\mathbf{g} \cdot \mathbf{d}_{nn'}) \frac{\partial \rho_n}{\partial P_n} \right] \mathbf{n}_{nn'} + \mathbf{q}_{nn'} \frac{\partial (\ln(\lambda_{nn'}))}{\partial P_n} \quad (39)$$

$$\begin{aligned} \frac{\partial \mathbf{q}_{nn'}}{\partial P_{n'}} &= \left[\frac{k_n k_{n'}}{k_n d_{n'} + k_{n'} d_n} \right] \lambda_{nn'} \left[-1 + \omega_n (\mathbf{g} \cdot \mathbf{d}_{nn'}) \frac{\partial \rho_{n'}}{\partial P_{n'}} \right] \mathbf{n}_{nn'} \\ &+ \mathbf{q}_{nn'} \frac{\partial (\ln(\lambda_{nn'}))}{\partial P_{n'}} \end{aligned} \quad (40)$$

620 **5.4 Numerical checks in VSFM**

621 VSFM uses a two-stage check to determine an acceptable numerical
 622 solution:

623 Stage-1: At any temporal integration stage, the model attempts to solve
 624 the set of nonlinear equations given by Equation (19) with a given
 625 timestep. If the model fails to find a solution to the nonlinear equations
 626 with a given error tolerance settings, the timestep is reduced by half and
 627 the model again attempts to solve the nonlinear problem. If the model
 628 fails to find a solution after a maximum number of time step cuts
 629 (currently 20), the model reports an error and stops execution. None of
 630 the simulations reported in this paper failed this check.

631 Stage-2: After a numerical solution for the nonlinear problem is obtained,
 632 a mass balance error is calculated as the difference between input and

Deleted: ¶

634 output fluxes and change in mass over the integration timestep. If the
635 mass balance error exceeds 10⁻⁵ kg m⁻², the error tolerances for the
636 nonlinear problem are tightened by a factor of 10 and the model re-enters
637 Stage-1. If the model fails to find a solution with an acceptable mass
638 balance error after 10 attempts of tightening error tolerances, the model
639 reports an error and stops execution. None of the simulations reported in
640 this paper failed this check.

641 **6 Code availability**

642 The standalone VFSM code is available at <https://github.com/MPP-LSM/MPP>. Notes
643 on how to run the VFSM for all benchmark problems and compare results against
644 PFLOTRAN at <https://bitbucket.org/gbisht/notes-for-gmd-2018-44>.

645 The research was performed using E3SM v1.0 and the code is available at
646 <https://github.com/E3SM-Project/E3SM>.

647 **7 Competing interests**

648 The authors declare that they have no conflict of interest.

649

650 **8 Acknowledgements**

651 This research was supported by the Director, Office of Science, Office of Biological
652 and Environmental Research of the US Department of Energy under contract no. DE-
653 AC02-05CH11231 as part of the Energy Exascale Earth System Model (E3SM)
654 programs.

655

656 **9 Tables**

657 **Table 1 Soil properties and discretization used in the three test problems**
 658 **described in section 2.3.**

Problem number	ϕ [-]	m [-]	α [Pa ⁻¹]	k [m ²]	dz [m]	dt [s]
1	0.368	0.5	3.4257x10 ⁻⁴	8.3913x10 ⁻¹²	<u>0.001</u>	<u>180</u>
2	0.4	0.54	4x10 ⁻⁴	2.5281x10 ⁻¹² (top layer)	<u>0.01</u>	<u>100</u>
		55		2.5281x10 ⁻¹³ (bottom layer)		
3	0.368	0.5	3.4257x10 ⁻⁴	8.3913x10 ⁻¹²	<u>0.01</u>	<u>3600</u>

Formatted Table
 Inserted Cells
 Inserted Cells

659

660 **Table 2 Bias, root mean square error (RMSE), and correlation (R²) between**
 661 **simulated water table depth and Fan et al. (2013) data.**

	Bias [m]	RMSE [m]	R²
For all grids in ELM simulation with default f_{drain}	-10.3	21.3	0.28
For all grids in ELM simulation with optimal f_{drain}	2.10	8.33	0.91
For 79% grids with optimal f_{drain} in ELM simulation with optimal f_{drain}	-0.04	0.67	0.99
For 21% grids without optimal f_{drain} in ELM simulation with optimal f_{drain}	-9.82	18.08	0.31

662

663

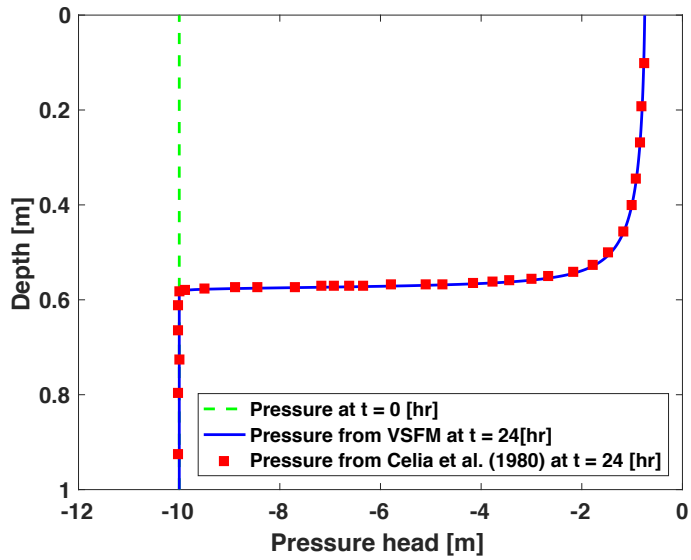
664 **Table 3 ILAMB benchmark scores for latent heat flux (LH), sensible heat flux**
 665 **(SH), total water storage anomaly (TWSA), and surface runoff. The calculation**
 666 **of ILAMB metrics and scores are described at <http://redwood.ess.uci.edu/>.**

	Data Source	Simulation with default f_d			Simulation with optimal f_d		
		Bias	RMSE	ILAMB Score	Bias	RMSE	ILAMB Score
LH	FLUXNET	10.1 [Wm ⁻²]	21.0 [Wm ⁻²]	0.68	9.5 [Wm ⁻²]	21.3 [Wm ⁻²]	0.68
	GBAF	7.1 [Wm ⁻²]	16.3 [Wm ⁻²]	0.81	6.3 [Wm ⁻²]	16.3 [Wm ⁻²]	0.81
SH	FLUXNET	6.7 [Wm ⁻²]	22.5 [Wm ⁻²]	0.66	7.1 [Wm ⁻²]	22.8 [Wm ⁻²]	0.65
	GBAF	6.9 [Wm ⁻²]	21.2 [Wm ⁻²]	0.71	7.6 [Wm ⁻²]	21.7 [Wm ⁻²]	0.70
TWSA	GRACE	1.3 [cm]	7.8 [cm]	0.48	3.0 [cm]	9.6 [cm]	0.48
Runoff	Dai	-0.26 [kg m ⁻² d ⁻¹]	0.91 [m ² m ⁻² d ⁻¹]	0.52	-0.23 [kg m ⁻² d ⁻¹]	0.88 [kg m ⁻² d ⁻¹]	0.50

667

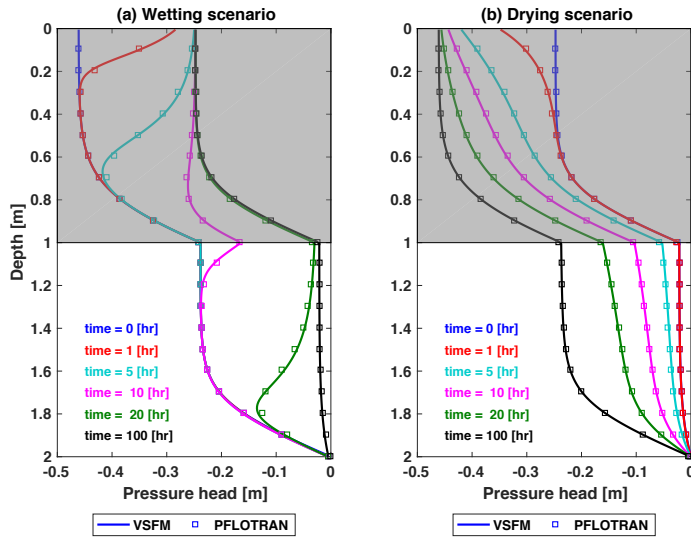
668

669 **10 Figures**



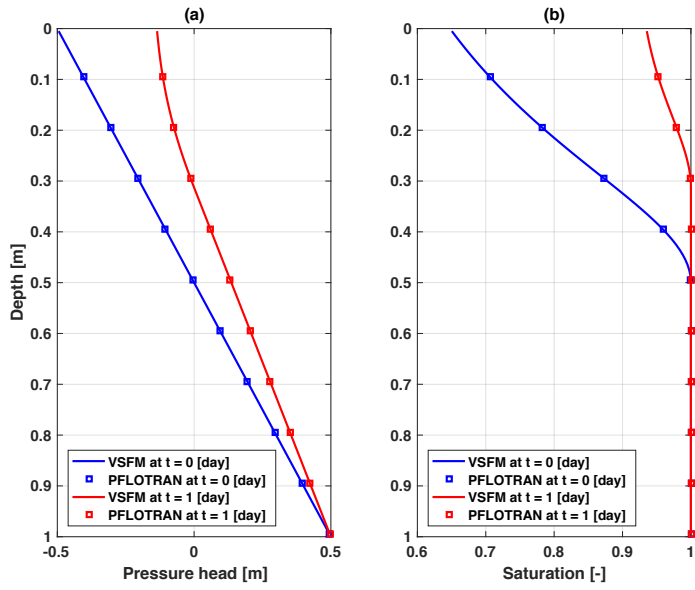
670

671 **Figure 1. Comparison of VSFM simulated pressure profile (blue line) against**
672 **data (red square) reported in Celia et al. (1990) at time = 24 hr for infiltration**
673 **in a dry soil column. Initial pressure condition is shown by green line.**



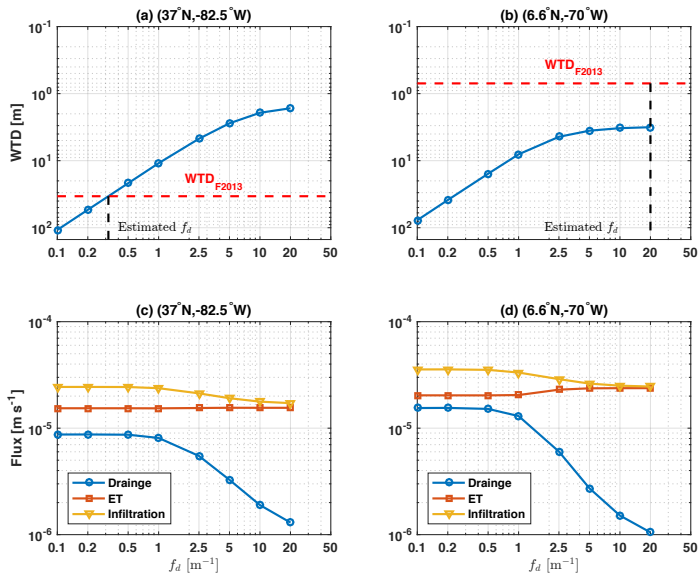
674

675 **Figure 2. Transient liquid pressure simulated for a two layer soil system by**
 676 **VFSM (solid line) and PFLOTRAN (square) for wetting (left) and drying (right)**
 677 **scenarios.**



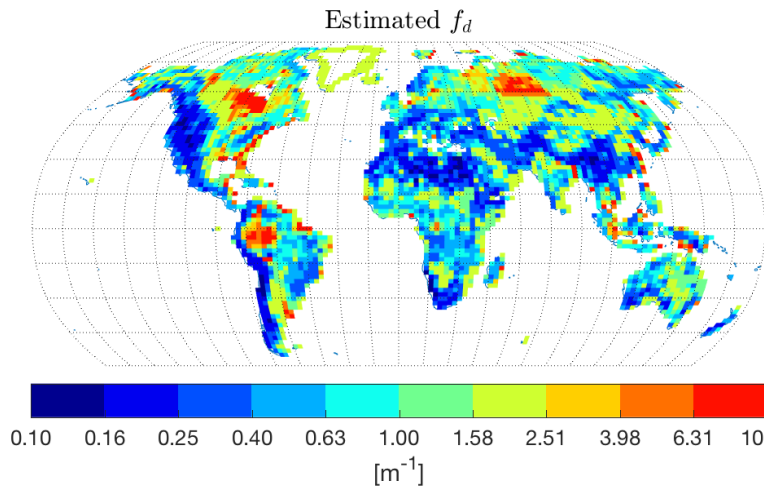
678

679 **Figure 3. Transient liquid pressure (a) and soil saturation (b) simulated by**
 680 **VSFM (solid line) and PFLOTRAN (square) for the water table dynamics test**
 681 **problem.**



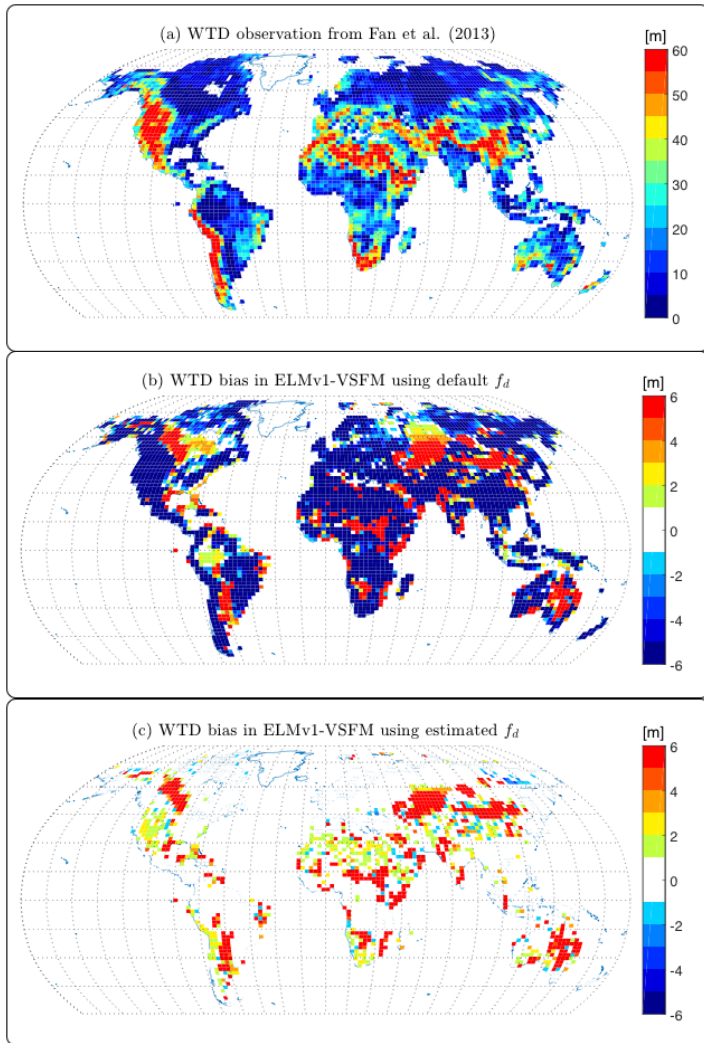
682
 683 **Figure 4. (a-b) The nonlinear relationship between simulated water table**
 684 **depth (WTD) and f_d for two gridcells within ELM's global grid. WTD from the**
 685 **Fan et al. (2013) dataset and optimal f_d for the two gridcells are shown with a**
 686 **dashed red and dashed black lines, respectively. (c-d) The simulated drainage,**
 687 **evapotranspiration, and infiltration fluxes as functions of optimal f_d for the**
 688 **two ELM gridcells.**

689



690

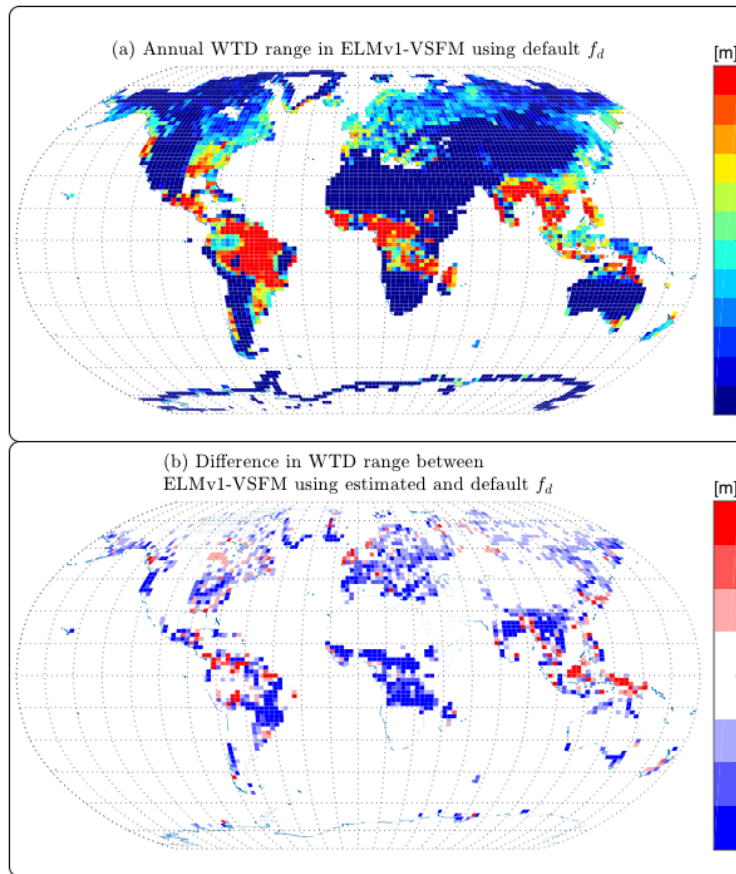
691 **Figure 5. Global estimate of f_d .**



692

693 **Figure 6. (a) Water table depth observation from Fan et al. (2013); (b) Water**
 694 **table depth biases (=Model - Obs) from ELMv1-VSFM using default spatially**
 695 **homogeneous f_d ; and (c) Water table depth biases from ELMv1-VSFM using**
 696 **spatially heterogeneous f_d .**

697



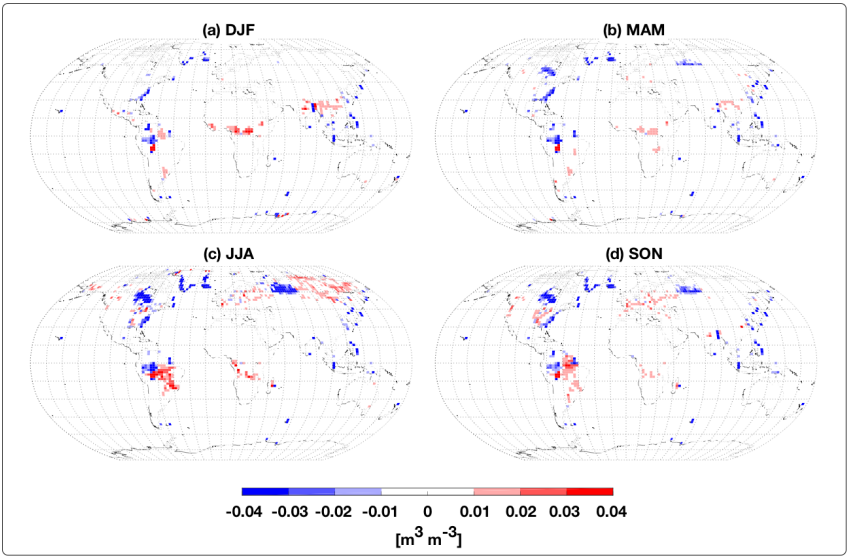
698

699 **Figure 7. (a) Annual range of water table depth for ELMv1-VSFM simulation**

700 **with spatially heterogeneous estimates of f_d and (b) Difference in annual**

701 **water table depth range between simulations with optimal and default f_d .**

702



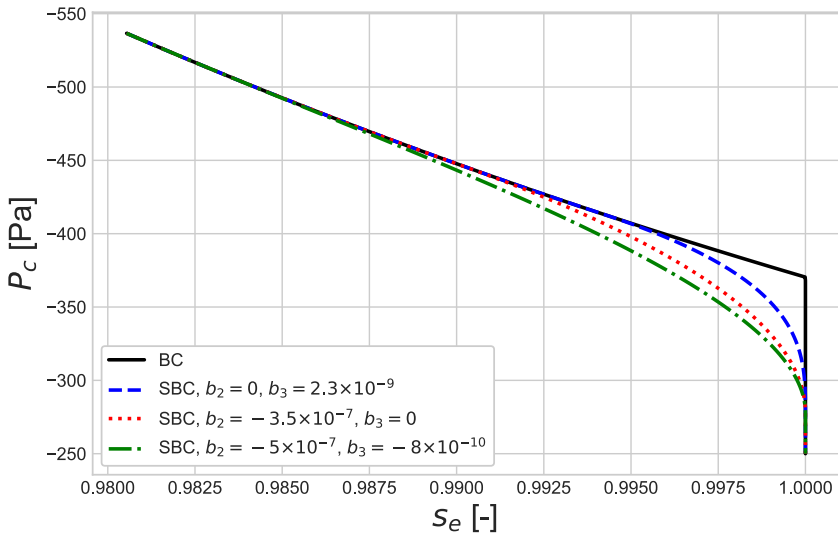
703

704 **Figure 8. Seasonal monthly mean soil moisture differences for top 10 cm**

705 **between ELMv1-VSFM simulations with optimal and default f_d values.**

706

707



708

709 **Figure A 1** The Brooks-Corey water rendition curve for estimating liquid saturation, s_e ,
710 as a function of capillary pressure, P_c , shown in solid black line and smooth
711 approximation of Brooks-Corey (SBC) are shown in dashed line.

712

713 **References**

- 714 Alkhaier, F., Flerchinger, G. N., and Su, Z.: Shallow groundwater effect on land surface
715 temperature and surface energy balance under bare soil conditions: modeling and
716 description, *Hydrol. Earth Syst. Sci.*, 16, 1817-1831, 2012.
- 717 Alley, W. M.: *Ground Water and Climate*, *Ground Water*, 39, 161-161, 2001.
- 718 Amenu, G. G. and Kumar, P.: A model for hydraulic redistribution incorporating
719 coupled soil-root moisture transport, *Hydrol. Earth Syst. Sci.*, 12, 55-74, 2008.
- 720 Anyah, R. O., Weaver, C. P., Miguez-Macho, G., Fan, Y., and Robock, A.: Incorporating
721 water table dynamics in climate modeling: 3. Simulated groundwater influence on
722 coupled land-atmosphere variability, *Journal of Geophysical Research: Atmospheres*,
723 113, n/a-n/a, 2008.
- 724 Balay, S., Abhyankar, S., Adams, M. F., Brown, J., Brune, P., Buschelman, K., Dalcin, L.,
725 Eijkhout, V., Gropp, W. D., Kaushik, D., Knepley, M. G., McInnes, L. C., Rupp, K., Smith,
726 B. F., Zampini, S., Zhang, H., and Zhang, H.: *PETSc Users Manual*, Argonne National
727 Laboratory ANL-95/11 - Revision 3.7, 1-241 pp., 2016.
- 728 Banks, E. W., Brunner, P., and Simmons, C. T.: Vegetation controls on variably
729 saturated processes between surface water and groundwater and their impact on the
730 state of connection, *Water Resources Research*, 47, n/a-n/a, 2011.
- 731 Bense, V. F., Kooi, H., Ferguson, G., and Read, T.: Permafrost degradation as a control
732 on hydrogeological regime shifts in a warming climate, *Journal of Geophysical
733 Research: Earth Surface*, 117, 2012.
- 734 Bernhardt, M., Schulz, K., Liston, G. E., and Zängl, G.: The influence of lateral snow
735 redistribution processes on snow melt and sublimation in alpine regions, *Journal of
736 Hydrology*, 424-425, 196-206, 2012.
- 737 Beven, K. J. and Kirkby, M. J.: A physically based, variable contributing area model of
738 basin hydrology / Un modèle à base physique de zone d'appel variable de l'hydrologie
739 du bassin versant, *Hydrological Sciences Bulletin*, 24, 43-69, 1979.
- 740 Bisht, G., Huang, M., Zhou, T., Chen, X., Dai, H., Hammond, G. E., Riley, W. J., Downs, J. L.,
741 Liu, Y., and Zachara, J. M.: Coupling a three-dimensional subsurface flow and transport
742 model with a land surface model to simulate stream-aquifer-land interactions
743 (CP v1.0), *Geosci. Model Dev.*, 10, 4539-4562, 2017.
- 744 Bisht, G., Riley, W. J., Wainwright, H. M., Dafflon, B., Yuan, F., and Romanovsky, V. E.:
745 Impacts of microtopographic snow redistribution and lateral subsurface processes
746 on hydrologic and thermal states in an Arctic polygonal ground ecosystem: a case
747 study using ELM-3D v1.0, *Geosci. Model Dev.*, 11, 61-76, 2018.
- 748 Bohrer, G., Mourad, H., Laursen, T. A., Drewry, D., Avissar, R., Poggi, D., Oren, R., and
749 Katul, G. G.: Finite element tree crown hydrodynamics model (FETCH) using porous
750 media flow within branching elements: A new representation of tree hydrodynamics,
751 *Water Resources Research*, 41, n/a-n/a, 2005.
- 752 Brooks, R. H. and Corey, A. T.: *Hydraulic properties of porous media*, Colorado State
753 University, Fort Collins, CO, 1964.
- 754 Brown, J., Knepley, M. G., May, D. A., McInnes, L. C., and Smith, B.: *Composable linear
755 solvers for multiphysics*, 2012, 55-62.
- 756 Brunke, M. A., Broxton, P., Pelletier, J., Gochis, D., Hazenberg, P., Lawrence, D. M.,
757 Leung, L. R., Niu, G.-Y., Troch, P. A., and Zeng, X.: *Implementing and Evaluating Variable*

758 Soil Thickness in the Community Land Model, Version 4.5 (CLM4.5), *Journal of*
759 *Climate*, 29, 3441-3461, 2016.

760 Celia, M. A., Bouloutas, E. T., and Zarba, R. L.: A general mass-conservative numerical
761 solution for the unsaturated flow equation, *Water Resources Research*, 26, 1483-
762 1496, 1990.

763 Chen, J. and Kumar, P.: Topographic Influence on the Seasonal and Interannual
764 Variation of Water and Energy Balance of Basins in North America, *Journal of Climate*,
765 14, 1989-2014, 2001.

766 Chen, X. and Hu, Q.: Groundwater influences on soil moisture and surface evaporation,
767 *Journal of Hydrology*, 297, 285-300, 2004.

768 Chen, Y., Chen, Y., Xu, C., Ye, Z., Li, Z., Zhu, C., and Ma, X.: Effects of ecological water
769 conveyance on groundwater dynamics and riparian vegetation in the lower reaches
770 of Tarim River, China, *Hydrological Processes*, 24, 170-177, 2010.

771 Clapp, R. B. and Hornberger, G. M.: Empirical equations for some soil hydraulic
772 properties, *Water Resources Research*, 14, 601-604, 1978.

773 Clark, M. P., Fan, Y., Lawrence, D. M., Adam, J. C., Bolster, D., Gochis, D. J., Hooper, R. P.,
774 Kumar, M., Leung, L. R., Mackay, D. S., Maxwell, R. M., Shen, C., Swenson, S. C., and Zeng,
775 X.: Improving the representation of hydrologic processes in Earth System Models,
776 *Water Resources Research*, 51, 5929-5956, 2015.

777 Collier, N., Hoffman, F. M., Lawrence, D. M., Keppel-Aleks, G., Koven, C. D., Riley, W.
778 J., Mu, M., and Randerson, J. T.: The International Land 1 Model Benchmarking
779 (ILAMB) System: Design, Theory, and Implementation, in review *J. Advances in*
780 *Modeling Earth Systems*, 2018. 2018.

781 Dai, A. and Trenberth, K. E.: Estimates of Freshwater Discharge from Continents:
782 Latitudinal and Seasonal Variations, *Journal of Hydrometeorology*, 3, 660-687, 2002.

783 Dams, J., Woldeamlak, S. T., and Batelaan, O.: Predicting land-use change and its
784 impact on the groundwater system of the Kleine Nete catchment, Belgium, *Hydrol.*
785 *Earth Syst. Sci.*, 12, 1369-1385, 2008.

786 Dennis, J. M., Vertenstein, M., Worley, P. H., Mirin, A. A., Craig, A. P., Jacob, R., and
787 Mickelson, S.: Computational performance of ultra-high-resolution capability in the
788 Community Earth System Model, *The International Journal of High Performance*
789 *Computing Applications*, 26, 5-16, 2012.

790 E3SM Project, D.: Energy Exascale Earth System Model. 2018.

791 Fan, Y., Li, H., and Miguez-Macho, G.: Global Patterns of Groundwater Table Depth,
792 *Science*, 339, 940-943, 2013.

793 Fan, Y., Miguez-Macho, G., Weaver, C. P., Walko, R., and Robock, A.: Incorporating
794 water table dynamics in climate modeling: 1. Water table observations and
795 equilibrium water table simulations, *Journal of Geophysical Research: Atmospheres*,
796 112, n/a-n/a, 2007.

797 Farthing, M. W., Kees, C. E., and Miller, C. T.: Mixed finite element methods and higher
798 order temporal approximations for variably saturated groundwater flow, *Advances*
799 *in Water Resources*, 26, 373-394, 2003.

800 Ferguson, I. M. and Maxwell, R. M.: Human impacts on terrestrial hydrology: climate
801 change versus pumping and irrigation, *Environmental Research Letters*, 7, 044022,
802 2012.

803 Frampton, A., Painter, S., Lyon, S. W., and Destouni, G.: Non-isothermal, three-phase
804 simulations of near-surface flows in a model permafrost system under seasonal
805 variability and climate change, *Journal of Hydrology*, 403, 352-359, 2011.

806 Ghimire, B., Riley, W. J., Koven, C. D., Mu, M., and Randerson, J. T.: Representing leaf
807 and root physiological traits in CLM improves global carbon and nitrogen cycling
808 predictions, *Journal of Advances in Modeling Earth Systems*, 8, 598-613, 2016.

809 Grant, R. F., Humphreys, E. R., and Lafleur, P. M.: Ecosystem CO₂ and CH₄ exchange in
810 a mixed tundra and a fen within a hydrologically diverse Arctic landscape: 1. Modeling
811 versus measurements, *Journal of Geophysical Research: Biogeosciences*, 120, 1366-
812 1387, 2015.

813 Grant, R. F., Mekonnen, Z. A., Riley, W. J., Wainwright, H. M., Graham, D., and Torn, M.
814 S.: Mathematical Modelling of Arctic Polygonal Tundra with Ecosys: 1.
815 Microtopography Determines How Active Layer Depths Respond to Changes in
816 Temperature and Precipitation, *Journal of Geophysical Research: Biogeosciences*,
817 122, 3161-3173, 2017.

818 Green, T. R., Taniguchi, M., Kooi, H., Gurdak, J. J., Allen, D. M., Hiscock, K. M., Treidel, H.,
819 and Aureli, A.: Beneath the surface of global change: Impacts of climate change on
820 groundwater, *Journal of Hydrology*, 405, 532-560, 2011.

821 Gutmann, E. D. and Small, E. E.: The effect of soil hydraulic properties vs. soil texture
822 in land surface models, *Geophysical Research Letters*, 32, 2005.

823 Hammond, G. E. and Lichtner, P. C.: Field-scale model for the natural attenuation of
824 uranium at the Hanford 300 Area using high-performance computing, *Water*
825 *Resources Research*, 46, n/a-n/a, 2010.

826 Hilberts, A. G. J., Troch, P. A., and Paniconi, C.: Storage-dependent drainable porosity
827 for complex hillslopes, *Water Resources Research*, 41, n/a-n/a, 2005.

828 Hoffman, F. M., Koven, C. D., Keppel-Aleks, G., Lawrence, D. M., Riley, W. J., Randerson,
829 J. T., Ahlstrom, A., Abramowitz, G., Baldocchi, D. D., Best, M. J., Bond-Lamberty, B.,
830 Kauwe}, M. G. D., Denning, A. S., Desai, A. R., Eyring, V., Fisher, J. B., Fisher, R. A.,
831 Gleckler, P. J., Huang, M., Hugelius, G., Jain, A. K., Kiang, N. Y., Kim, H., Koster, R. D.,
832 Kumar, S. V., Li, H., Luo, Y., Mao, J., McDowell, N. G., Mishra, U., Moorcroft, P. R., Pau, G.
833 S. H., Ricciuto, D. M., Schaefer, K., Schwalm, C. R., Serbin, S. P., Shevliakova, E., Slater,
834 A. G., Tang, J., Williams, M., Xia, J., Xu, C., Joseph, R., and Koch, D.: International Land
835 Model Benchmarking (ILAMB) 2016 Workshop Report, U.S. Department of Energy,
836 Office of Science, 159 pp., 2017.

837 Hou, Z., Huang, M., Leung, L. R., Lin, G., and Ricciuto, D. M.: Sensitivity of surface flux
838 simulations to hydrologic parameters based on an uncertainty quantification
839 framework applied to the Community Land Model, *Journal of Geophysical Research:*
840 *Atmospheres*, 117, n/a-n/a, 2012.

841 Hwang, T., Band, L. E., Vose, J. M., and Tague, C.: Ecosystem processes at the watershed
842 scale: Hydrologic vegetation gradient as an indicator for lateral hydrologic
843 connectivity of headwater catchments, *Water Resources Research*, 48, n/a-n/a, 2012.

844 Ji, P., Yuan, X., and Liang, X.-Z.: Do Lateral Flows Matter for the Hyperresolution Land
845 Surface Modeling?, *Journal of Geophysical Research: Atmospheres*, doi:
846 10.1002/2017JD027366, 2017. n/a-n/a, 2017.

847 Jiang, X., Niu, G.-Y., and Yang, Z.-L.: Impacts of vegetation and groundwater dynamics
848 on warm season precipitation over the Central United States, *Journal of Geophysical*
849 *Research: Atmospheres*, 114, n/a-n/a, 2009.

850 Jung, M., Reichstein, M., and Bondeau, A.: Towards global empirical upscaling of
851 FLUXNET eddy covariance observations: validation of a model tree ensemble
852 approach using a biosphere model, *Biogeosciences*, 6, 2001-2013, 2009.

853 Kane, D. L., Hinkel, K. M., Goering, D. J., Hinzman, L. D., and Outcalt, S. I.: Non-
854 conductive heat transfer associated with frozen soils, *Global and Planetary Change*,
855 29, 275-292, 2001.

856 Kees, C. E. and Miller, C. T.: Higher order time integration methods for two-phase flow,
857 *Advances in Water Resources*, 25, 159-177, 2002.

858 Kim, H., Yeh, P. J. F., Oki, T., and Kanae, S.: Role of rivers in the seasonal variations of
859 terrestrial water storage over global basins, *Geophysical Research Letters*, 36, n/a-
860 n/a, 2009.

861 Kollet, S. J. and Maxwell, R. M.: Capturing the influence of groundwater dynamics on
862 land surface processes using an integrated, distributed watershed model, *Water*
863 *Resources Research*, 44, n/a-n/a, 2008.

864 Koster, R. D., Suarez, M. J., Ducharne, A., Stieglitz, M., and Kumar, P.: A catchment-
865 based approach to modeling land surface processes in a general circulation model: 1.
866 Model structure, *Journal of Geophysical Research: Atmospheres*, 105, 24809-24822,
867 2000.

868 Kundzewicz, Z. W. and Doli, P.: Will groundwater ease freshwater stress under climate
869 change?, *Hydrological Sciences Journal*, 54, 665-675, 2009.

870 Lasslop, G., Reichstein, M., Papale, D., Richardson, A. D., Arneeth, A., Barr, A., Stoy, P.,
871 and Wohlfahrt, G.: Separation of net ecosystem exchange into assimilation and
872 respiration using a light response curve approach: critical issues and global
873 evaluation, *Global Change Biology*, 16, 187-208, 2010.

874 Leng, G., Huang, M., Tang, Q., and Leung, L. R.: A modeling study of irrigation effects
875 on global surface water and groundwater resources under a changing climate, *Journal*
876 *of Advances in Modeling Earth Systems*, 7, 1285-1304, 2015.

877 Leng, G., Leung, L. R., and Huang, M.: Significant impacts of irrigation water sources
878 and methods on modeling irrigation effects in the ACMEland Model, *Journal of*
879 *Advances in Modeling Earth Systems*, 9, 1665-1683, 2017.

880 Leung, L. R., Huang, M., Qian, Y., and Liang, X.: Climate-soil-vegetation control on
881 groundwater table dynamics and its feedbacks in a climate model, *Climate Dynamics*,
882 36, 57-81, 2011.

883 Levine, J. B. and Salvucci, G. D.: Equilibrium analysis of groundwater-vadose zone
884 interactions and the resulting spatial distribution of hydrologic fluxes across a
885 Canadian Prairie, *Water Resources Research*, 35, 1369-1383, 1999.

886 Liang, X., Xie, Z., and Huang, M.: A new parameterization for surface and groundwater
887 interactions and its impact on water budgets with the variable infiltration capacity
888 (VIC) land surface model, *Journal of Geophysical Research: Atmospheres*, 108, n/a-
889 n/a, 2003.

890 Lohse, K. A., Brooks, P. D., McIntosh, J. C., Meixner, T., and Huxman, T. E.: Interactions
891 Between Biogeochemistry and Hydrologic Systems, *Annual Review of Environment*
892 *and Resources*, 34, 65-96, 2009.

893 Manoli, G., Bonetti, S., Domec, J.-C., Putti, M., Katul, G., and Marani, M.: Tree root
894 systems competing for soil moisture in a 3D soil-plant model, *Advances in Water*
895 *Resources*, 66, 32-42, 2014.

896 Marvel, K., Biasutti, M., Bonfils, C., Taylor, K. E., Kushnir, Y., and Cook, B. I.: Observed
897 and Projected Changes to the Precipitation Annual Cycle, *Journal of Climate*, 30, 4983-
898 4995, 2017.

899 Maxwell, R. M. and Miller, N. L.: Development of a Coupled Land Surface and
900 Groundwater Model, *Journal of Hydrometeorology*, 6, 233-247, 2005.

901 McDowell, N. G. and Allen, C. D.: Darcy's law predicts widespread forest mortality
902 under climate warming, *Nature Clim. Change*, 5, 669-672, 2015.

903 Miguez-Macho, G., Fan, Y., Weaver, C. P., Walko, R., and Robock, A.: Incorporating
904 water table dynamics in climate modeling: 2. Formulation, validation, and soil
905 moisture simulation, *Journal of Geophysical Research: Atmospheres*, 112, n/a-n/a,
906 2007.

907 Milly, P. C. D., Malyshev, S. L., Shevliakova, E., Dunne, K. A., Findell, K. L., Gleeson, T.,
908 Liang, Z., Philipps, P., Stouffer, R. J., and Swenson, S.: An Enhanced Model of Land
909 Water and Energy for Global Hydrologic and Earth-System Studies, *Journal of*
910 *Hydrometeorology*, 15, 1739-1761, 2014.

911 Mualem, Y.: A new model for predicting the hydraulic conductivity of unsaturated
912 porous media, *Water Resources Research*, 12, 513-522, 1976.

913 Niu, G.-Y., Yang, Z.-L., Dickinson, R. E., and Gulden, L. E.: A simple TOPMODEL-based
914 runoff parameterization (SIMTOP) for use in global climate models, *Journal of*
915 *Geophysical Research: Atmospheres*, 110, n/a-n/a, 2005.

916 Niu, G.-Y., Yang, Z.-L., Dickinson, R. E., Gulden, L. E., and Su, H.: Development of a simple
917 groundwater model for use in climate models and evaluation with Gravity Recovery
918 and Climate Experiment data, *Journal of Geophysical Research: Atmospheres*, 112,
919 n/a-n/a, 2007.

920 Niu, J., Shen, C., Chambers, J. Q., Melack, J. M., and Riley, W. J.: Interannual Variation in
921 Hydrologic Budgets in an Amazonian Watershed with a Coupled Subsurface-Land
922 Surface Process Model, *Journal of Hydrometeorology*, 18, 2597-2617, 2017.

923 Oleson, K. W., D.M. Lawrence, G.B. Bonan, B. Drewniak, M. Huang, C.D. Koven, S. Levis,
924 F. Li, W.J. Riley, Z.M. Subin, S.C. Swenson, P.E. Thornton, A. Bozbiyik, R. Fisher, E.
925 Kluzek, J.-F. Lamarque, P.J. Lawrence, L.R. Leung, W. Lipscomb, S. Muszala, D.M.
926 Ricciuto, W. Sacks, Y. Sun, J. Tang, Z.-L. Yang: Technical Description of version 4.5 of
927 the Community Land Model (CLM), National Center for Atmospheric Research,
928 Boulder, CO, 422 pp., 2013.

929 Pacific, V. J., McGlynn, B. L., Riveros-Iregui, D. A., Welsch, D. L., and Epstein, H. E.:
930 Landscape structure, groundwater dynamics, and soil water content influence soil
931 respiration across riparian-hillslope transitions in the Tenderfoot Creek
932 Experimental Forest, Montana, *Hydrological Processes*, 25, 811-827, 2011.

933 Pelletier, J. D., Broxton, P. D., Hazenberg, P., Zeng, X., Troch, P. A., Niu, G.-Y., Williams,
934 Z., Brunke, M. A., and Gochis, D.: A gridded global data set of soil, intact regolith, and
935 sedimentary deposit thicknesses for regional and global land surface modeling,
936 *Journal of Advances in Modeling Earth Systems*, 8, 41-65, 2016.

937 Petra, D.: Vulnerability to the impact of climate change on renewable groundwater
938 resources: a global-scale assessment, *Environmental Research Letters*, 4, 035006,
939 2009.

940 Piao, S. L., Ito, A., Li, S. G., Huang, Y., Ciais, P., Wang, X. H., Peng, S. S., Nan, H. J., Zhao, C.,
941 Ahlström, A., Andres, R. J., Chevallier, F., Fang, J. Y., Hartmann, J., Huntingford, C., Jeong,
942 S., Levis, S., Levy, P. E., Li, J. S., Lomas, M. R., Mao, J. F., Mayorga, E., Mohammat, A.,
943 Muraoka, H., Peng, C. H., Peylin, P., Poulter, B., Shen, Z. H., Shi, X., Sitch, S., Tao, S., Tian,
944 H. Q., Wu, X. P., Xu, M., Yu, G. R., Viogy, N., Zaehle, S., Zeng, N., and Zhu, B.: The carbon
945 budget of terrestrial ecosystems in East Asia over the last two decades,
946 *Biogeosciences*, 9, 3571-3586, 2012.

947 Pruess, K., Oldenburg, C., and Moridis, G.: TOUGH2 User's Guide, Version 2.0,
948 Lawrence Berkeley National Laboratory, Berkeley, CALBNL-43134, 1999.

949 Rihani, J. F., Maxwell, R. M., and Chow, F. K.: Coupling groundwater and land surface
950 processes: Idealized simulations to identify effects of terrain and subsurface
951 heterogeneity on land surface energy fluxes, *Water Resources Research*, 46, n/a-n/a,
952 2010.

953 Salvucci, G. D. and Entekhabi, D.: Hillslope and Climatic Controls on Hydrologic Fluxes,
954 *Water Resources Research*, 31, 1725-1739, 1995.

955 Shen, C., Niu, J., and Phanikumar, M. S.: Evaluating controls on coupled hydrologic and
956 vegetation dynamics in a humid continental climate watershed using a subsurface-
957 land surface processes model, *Water Resources Research*, 49, 2552-2572, 2013.

958 Siebert, S., Burke, J., Faures, J. M., Frenken, K., Hoogeveen, J., Döll, P., and Portmann, F.
959 T.: Groundwater use for irrigation – a global inventory, *Hydrol. Earth Syst. Sci.*, 14,
960 1863-1880, 2010.

961 Sivapalan, M., Beven, K., and Wood, E. F.: On hydrologic similarity: 2. A scaled model
962 of storm runoff production, *Water Resources Research*, 23, 2266-2278, 1987.

963 Soylu, M. E., Istanbuluoglu, E., Lenters, J. D., and Wang, T.: Quantifying the impact of
964 groundwater depth on evapotranspiration in a semi-arid grassland region, *Hydrol.*
965 *Earth Syst. Sci.*, 15, 787-806, 2011.

966 Sperry, J. S., Adler, F. R., Campbell, G. S., and Comstock, J. P.: Limitation of plant water
967 use by rhizosphere and xylem conductance: results from a model, *Plant, Cell &*
968 *Environment*, 21, 347-359, 1998.

969 Srivastava, R. and Yeh, T. C. J.: Analytical solutions for one-dimensional, transient
970 infiltration toward the water table in homogeneous and layered soils, *Water*
971 *Resources Research*, 27, 753-762, 1991.

972 Swenson, S. C. and Lawrence, D. M.: Assessing a dry surface layer-based soil resistance
973 parameterization for the Community Land Model using GRACE and FLUXNET-MTE
974 data, *Journal of Geophysical Research: Atmospheres*, 119, 10,299-210,312, 2014.

975 Swenson, S. C., Lawrence, D. M., and Lee, H.: Improved simulation of the terrestrial
976 hydrological cycle in permafrost regions by the Community Land Model, *Journal of*
977 *Advances in Modeling Earth Systems*, 4, n/a-n/a, 2012.

978 Tanaka, M., Girard, G., Davis, R., Peuto, A., and Bignell, N.: Recommended table for the
979 density of water between 0 °C and 40 °C based on recent experimental reports,
980 *Metrologia*, 38, 301, 2001.

981 Taylor, K. E., Stouffer, R. J., and Meehl, G. A.: An Overview of CMIP5 and the Experiment
982 Design, *Bulletin of the American Meteorological Society*, 93, 485-498, 2012.

983 Taylor, R. G., Scanlon, B., Döll, P., Rodell, M., Van Beek, R., Wada, Y., Longuevergne, L.,
984 Leblanc, M., Famiglietti, J. S., and Edmunds, M.: Ground water and climate change,
985 Nature Climate Change, 3, 322-329, 2013.
986 Tian, W., Li, X., Cheng, G. D., Wang, X. S., and Hu, B. X.: Coupling a groundwater model
987 with a land surface model to improve water and energy cycle simulation, Hydrol.
988 Earth Syst. Sci., 16, 4707-4723, 2012.
989 van Genuchten, M. T.: A Closed-form Equation for Predicting the Hydraulic
990 Conductivity of Unsaturated Soils¹, Soil Science Society of America Journal, 44, 892-
991 898, 1980.
992 Walko, R. L., Band, L. E., Baron, J., Kittel, T. G. F., Lammers, R., Lee, T. J., Ojima, D., Sr., R.
993 A. P., Taylor, C., Tague, C., Tremback, C. J., and Vidale, P. L.: Coupled Atmosphere-
994 Biophysics-Hydrology Models for Environmental Modeling, Journal of Applied
995 Meteorology, 39, 931-944, 2000.
996 White, M. and STOMP, O. M.: Subsurface transport over multiple phases; Version 2.0;
997 Theory Guide, Pacific Northwest National Laboratory, 2000. 2000.
998 Yeh, P. J.-F. and Eltahir, E. A. B.: Representation of Water Table Dynamics in a Land
999 Surface Scheme. Part I: Model Development, Journal of Climate, 18, 1861-1880, 2005.
1000 York, J. P., Person, M., Gutowski, W. J., and Winter, T. C.: Putting aquifers into
1001 atmospheric simulation models: an example from the Mill Creek Watershed,
1002 northeastern Kansas, Advances in Water Resources, 25, 221-238, 2002.
1003 Yuan, X., Xie, Z., Zheng, J., Tian, X., and Yang, Z.: Effects of water table dynamics on
1004 regional climate: A case study over east Asian monsoon area, Journal of Geophysical
1005 Research: Atmospheres, 113, n/a-n/a, 2008.
1006 Zektser, I. S. and Everitt, L. G.: Groundwater resources of the world and their use,
1007 United Nations Educational, Scientific and Cultural Organization⁷, place de Fontenoy,
1008 75352 Paris 07 SP, 2004.
1009 Zeng, X. and Decker, M.: Improving the Numerical Solution of Soil Moisture-Based
1010 Richards Equation for Land Models with a Deep or Shallow Water Table, Journal of
1011 Hydrometeorology, 10, 308-319, 2009.
1012 Zhu, Q., Riley, W. J., Tang, J., and Koven, C. D.: Multiple soil nutrient competition
1013 between plants, microbes, and mineral surfaces: model development,
1014 parameterization, and example applications in several tropical forests,
1015 Biogeosciences, 13, 341-363, 2016.
1016
1017